ARL-TR-9869 ● JAN 2024

On Simulating the Pyroprobe-Induced Pyrolysis of Hydrocarbons with a Model Having a Detailed Finite-Rate Chemical Kinetics Mechanism: Results for 1,5,9-Decatriene

by Michael McQuaid, Chiung-Chu Chen, Rose Pesce-Rodriguez, Christopher Stone, Rodger Cornell

NOTICES

Disclaimers

The findings in this report are not to be construed as an official Department of the Army position unless so designated by other authorized documents.

Citation of manufacturer's or trade names does not constitute an official endorsement or approval of the use thereof.

Destroy this report when it is no longer needed. Do not return it to the originator.

ARL-TR-9869 ● JAN 2024

On Simulating the Pyroprobe-Induced Pyrolysis of Hydrocarbons with a Model Having a Detailed Finite-Rate Chemical Kinetics Mechanism: Results for 1,5,9-Decatriene

Michael McQuaid, Chiung-Chu Chen, Rose Pesce-Rodriguez, Christopher Stone, Rodger Cornell
DEVCOM Army Research Laboratory

REPORT DOCUMENTATION PAGE

1. REPORT DATE	2. REPORT TYPE	3. DATES COVERED	
		START DATE	END DATE
January 2024	Technical Report	October 2022	November 2023

4. TITLE AND SUBTITLE
On Simulating the Pyroprobe-Induced Pyrolysis of Hydrocarbons with a Model Having a Detailed Finite-Rate Chemical Kinetics Mechanism: Results for 1,5,9-Decatriene

5a. CONTRACT NUMBER	5b. GRANT NUMBER	5c. PROGRAM ELEMENT NUMBER
5d. PROJECT NUMBER	**5e. TASK NUMBER**	**5f. WORK UNIT NUMBER**

6. AUTHOR(S)
Michael McQuaid, Chiung-Chu Chen, Rose Pesce-Rodriguez, Christopher Stone, and Rodger Cornell

7. PERFORMING ORGANIZATION NAME(S) AND ADDRESS(ES)
DEVCOM Army Research Laboratory
ATTN: FCDD-RLA-WC
Aberdeen Proving Ground, MD 21005

8. PERFORMING ORGANIZATION REPORT NUMBER
ARL-TR-9869

9. SPONSORING/MONITORING AGENCY NAME(S) AND ADDRESS(ES)	10. SPONSOR/MONITOR'S ACRONYM(S)	11. SPONSOR/MONITOR'S REPORT NUMBER(S)

12. DISTRIBUTION/AVAILABILITY STATEMENT
DISTRIBUTION STATEMENT A. Approved for public release: distribution unlimited.

13. SUPPLEMENTARY NOTES
ORCID ID(s): Michael McQuaid, 0000-0001-5523-7468; Chiung-Chu Chen, 0000-0002-8666-9949; Christopher Stone, 0000-0002-9621-5334; Rodger Cornell, 0000-0003-1367-7443

14. ABSTRACT
As part of a program to develop and apply machine learning (ML) methods with the potential to significantly reduce the time and cost needed to create detailed finite-rate chemical kinetics mechanisms, we sought to demonstrate a capacity to model the pyroprobe-induced pyrolysis of hydrocarbons with eight or more carbon atoms. A homogeneous reactor model was formulated to represent the process. It was coupled with a chemical kinetics mechanism developed to represent the pyrolytic decomposition of 1,5,9-decatriene and employed to simulate a set of desorption/pyrolysis–gas-chromatography/mass spectroscopy (D/P–GC/MS) experiments whose results were previously reported. Although there were some discrepancies between measurement-derived and model-predicted concentrations of pyrolysis products that remain to be resolved, the overall agreement between the results indicated that the mechanism–model combination was sufficiently representative of the process to warrant use for ML model training. In addition, the model's results for the temporal dynamics of the experiments were analyzed, and insights were obtained that could be exploited to design D/P–GC/MS heating protocols that better probe the decomposition chemistry of interest.

15. SUBJECT TERMS
Weapons Sciences, pyrolysis, chemical kinetics, gas chromatography, physics-based modeling

16. SECURITY CLASSIFICATION OF:			17. LIMITATION OF ABSTRACT	18. NUMBER OF PAGES
a. REPORT	b. ABSTRACT	C. THIS PAGE		
UNCLASSIFIED	UNCLASSIFIED	UNCLASSIFIED	UU	54

19a. NAME OF RESPONSIBLE PERSON	19b. PHONE NUMBER *(Include area code)*
Michael McQuaid	(410) 278-6185

STANDARD FORM 298 (REV. 5/2020)
Prescribed by ANSI Std. Z39.18

Contents

List of Figures

List of Tables

Acknowledgments

We are grateful to Dr Josh Orlicki (ARL), who established via nuclear magnetic resonance the percentages of cis- and trans-1,5,9-decatriene conformers in the commercial sample employed in the experiments performed for this study. Funding for the study was provided by an ARL mission program titled “Machine Learning to Accelerate Detailed Finite-Rate Chemical Kinetics Mechanisms Creation for Continuum-Level Modeling of Energetic Material Decomposition and Combustion.” The simulations were run on a DoD High Performance Computing Modernization Program platform.

1. Introduction

Funded via a US Army Combat Capabilities Development Command Army Research Laboratory mission program titled "Machine Learning to Accelerate Detailed Finite-Rate Chemical Kinetics Mechanisms Creation for Continuum-Level Modeling of Energetic Material Decomposition and Combustion," we are investigating methods with the potential to significantly reduce the time and cost needed to create said mechanisms. The approach formulated to achieve that objective is predicated on employing solutions to "simple" thermochemical kinetics problems as bases for training machine learning (ML) frameworks to rank the relative importance of elementary chemical reactions that a reaction enumerator generates for an application. Among the applications for which predictive mechanism–model combinations are being sought are high-throughput analytical techniques employed for energetic material (EM) screening, including differential scanning calorimetry (Clay and Banning 2020), thermogravimetric analysis (Rozumov et al. 2020), and desorption/pyrolysis–gas-chromatography/mass spectrometry (D/P–GC/MS) (Pesce-Rodriguez et al. 2023). Requiring relatively small (1 mg) samples, such techniques are among the first to be employed to characterize an EM's thermal stability and the products of its pyrolysis. However, although the responses of EMs to the conditions created by these techniques are largely governed by thermochemical kinetics, and an elucidation of those kinetics might provide insights that would be useful in predicting an EM's potential to be fielded, there have been few (published) studies in which models with detailed finite-rate chemical kinetics mechanisms have been developed and implemented for that purpose.

In the case of D/P-GC/MS experiments, which were the focus of the study summarized herein, "pyroprobe" reactors provide a means for volatilizing samples whose vapor pressure at the temperature at which the GC/MS's injector will initially be set are below the instrument's detection threshold. Solid rocket and gun propellants, explosives, and most of the ingredients composing them are studied in this manner. However, a Web of Science search prompted by "pyroprobe/pyro-probe/pyro probe" yielded 210 citations, while "pyroprobe/pyro-probe/pyro probe and kinetics" yielded only 34 citations. And of those 34, only one (Lin et al. 2009) represented the chemical kinetics at a level of detail approaching that necessary to achieve the objectives to which we aspire. Cited more than 500 times, it suggests the potential for models with detailed finite-rate chemical kinetics mechanisms to increase the amount of information that can be derived from D/P–GC/MS experiments.

The dearth of studies comparable to that of Lin et al. is due in large part to two issues. One, which is alluded to above, is the time and cost required to develop and validate a detailed finite-rate chemical kinetics mechanism for an EM ingredient or formulation (regardless of phase) for which one does not already exist. The other is the lack of experimental techniques for probing the decomposition of an undiluted condensed-phase EM that can elucidate the chemical kinetics at the level of detail achievable with standard techniques for probing the decomposition and combustion of gas-phase systems. (Examples of the latter include jet-stirred reactors, plug-flow reactors, and shock tubes.) Under our program, we are seeking to develop and apply practical approaches that overcome these issues.

Herein, we summarize the formulation and validation of a homogeneous reactor (HR) model for simulating D/P–GC/MS experiments. As discussed previously (Chen et al. 2023a; Pesce-Rodriguez et al. 2023), toward developing and validating a framework that can be employed to model D/P-GC/MS experiments involving EM formulations with polymeric ingredients such as hydroxyl-terminated polybutadiene (HTPB) and nitrocellulose (NC), we sought as a test case a relatively inexpensive, commercially available hydrocarbon with a well-defined molecular structure having from 8 to 20 carbon atoms that like HTPB had cis, trans, and vinyl C=C groups. In addition, the compound had to be one for which we either had or could readily develop a (sub)network for decomposing the parent molecule. 1,5,9-decatriene (DTE, $C_{10}H_{16}$) appeared to meet these criteria. (The development of a mechanism for modeling its pyrolysis proved to require more effort than we anticipated [Chen et al. 2023a].)

Results generated by D/P–GC/MS experiments in which DTE samples were rapidly heated to a temperature ranging from 175 to 1000 °C were previously analyzed and reported (Pesce-Rodriguez et al. 2023). Posing demanding tests of a model's capacity to represent such experiments, they were simulated with the HR model. Comparisons of the model's predictions to measured results are presented and discussed. Some discrepancies were observed that remain to be resolved. (We proffer some speculation as to their source.) However, overall, the comparisons suggested that the mechanism–model combination was sufficiently representative of the process to warrant use for ML model training. Recommendations for simulation results that could be employed for that purpose are proffered and discussed.

2. Experimental Apparatus and Procedures

2.1 Review of Prior Experiments

A detailed description of the D/P-GC/MS apparatus and the procedures employed to identify and quantify the products generated by the pyroprobe-induced pyrolysis of DTE was provided previously (Pesce-Rodriguez et al. 2023). For convenience, we review here those aspects of the experiments that were pertinent to formulating a model to simulate them. DTE (>95% purity, CAS no.: 13393-64-1) was purchased from a commercial vendor (VWR) and employed as received. Comprising a mixture of 5Z (cis) and 5E (trans) conformers whose composition was reported by the vendor to be nearly 50% cis and 50% trans, it is a liquid at 20 °C and 1 atm. Its normal boiling point is reported to be 170 °C (Bykov 2004).

Samples were heated via a CDS Analytical Model 2000 Pyroprobe (coil type) that was connected to a GC/MS via a heated interface chamber. A schematic of the pyroprobe is shown in Fig. 1. A sample weighing approximately 1 mg was placed on a small plug of quartz wool and inserted into a 25-mm-long, 2.5-mm-inner-diameter (ID)* quartz tube. The tube, in turn, was inserted into the interior of the heating coil. The chamber had a 50 mL/min flow of 22.3 psia (1.52 atm) helium (He) passing through it (and over the pyroprobe) at all times. Its temperature at the start of each experiment was 175 °C. The energization of the heating coil raised the temperature of the tube's contents at 1000 °C/s to a set-point temperature (T_{sp}) in the range from 500 to 1000 °C. (An experiment in which the heating coil was not energized was also conducted; its T_{sp} was effectively 175 °C.) T_{sp} values were maintained for 20 s. The values were not independently measured. They were based on a calibration provided by the vendor.

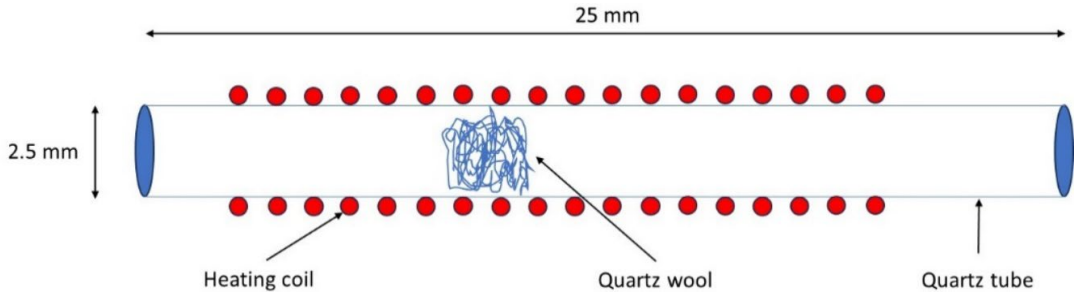

Fig. 1 Pyroprobe schematic

* In Pesce-Rodriguez et al. (2023), the ID of the quartz tube was reported to be 5 mm. That value is not correct. We also note that the quartz wool plug tended to be located slightly off-center toward the end of the tube that was slightly more constricted. Formulated based on the assumption that the properties of the gas within the tube were homogeneous, the model did not take this factor into account. We note it because it could be relevant to rationalizing discrepancies between measured and predicted results.

2.2 Additional Experiments

In the chromatograms presented by Pesce-Rodriguez et al. (2023), there was some question as to the source/assignment of "peak 15." It was a prominent feature in every chromatogram produced, and it was unquestionably attributable to DTE. However, it preceded (in time) a much larger feature ("peak 18") that was also unquestionably attributable DTE. Based on the results of some experiments that were not reported, peak 15 was attributed to DTE in the headspace prior to the heating coil's energization while peak 18 was attributed to DTE desorbed from the quartz wool after the coil was energized.

Reanalyzing the results for this study, the first author thought it possible that peak 15 might in fact be attributable to cis-DTE and peak 18 attributable to trans-DTE. To appraise that possibility, Dr Pesce-Rodriguez diluted a sample of the vendor-supplied DTE with isopropanol and directly introduced the mixture into the GC's injector. The chromatogram that resulted is shown in Fig. 2. It makes clear that the column retention times for cis- and trans-DTE were effectively identical, corroborating the attribution of peak 15 to DTE in the headspace prior to the heating coil's energization.

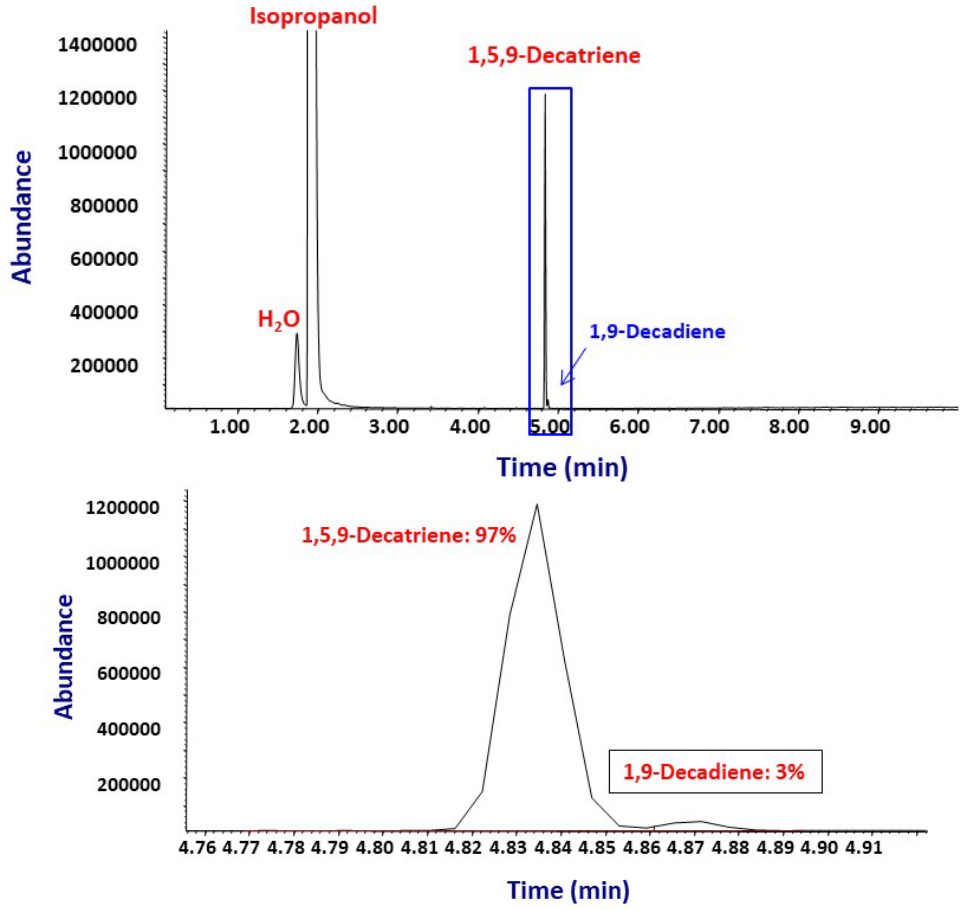

Fig. 2 Chromatogram of DTE-isopropanol mixture: direct injection

It was also observed that, in contrast to the prior study, where seven organic compounds besides DTE were observed in every chromatogram and whose source was assumed to be the vendor-supplied sample, the only measurable (organic) impurity in the mixture was 1,9-decadiene. We are at a loss to explain the source of the other six. However, observing that the chromatogram features attributable to these species were present and did not vary significantly relative to one another at each of the four set-point temperatures, we concluded that, like peak 15, they were in the headspace prior to the coil being energized and were not pyrolyzed to any significant extent. Thus, they were omitted from consideration in the analysis.

In addition, (gas-phase) equilibrium calculations based on the thermodynamic database of the chemical kinetics mechanism employed for this study led the first author to think that trans-DTE's concentration in a liquid sample at 298 K would be a factor of 5 or more greater than cis-DTE's, and therefore questioned VWR's 50% cis - 50% trans estimate. However, their estimate was (effectively) confirmed by a nuclear magnetic resonance (NMR) spectrum recorded by Dr Josh Orlicki, who found the VWR-supplied sample to be 52% cis-DTE and 48% trans-DTE.

Although the first author was surprised by the large discrepancy between the measured ratio and the equilibrium prediction, it could be rationalized. In developing the DTE mechanism employed for this study, Dr Chen found the barrier to the interconversion between the two conformers via a rotation about the C=C bond to be about 70 kcal/mol. Therefore, if the synthesis procedure employed to make the sample slightly favored the formation of cis conformers, the cis:trans ratio it engendered might not significantly change over a years-long period of time if the sample's temperature was maintained in the neighborhood of 25 °C.

3. Computational Methods

3.1 HR Model Formulation

Although the tube containing the sample was open at both ends, we thought its length vs. ID offered sufficient confinement of the gases within it to idealize the volume (V) as an HR. Moreover, the volume's coupling to the reservoir of He in which the tube was immersed would maintain the pressure (P) of those gases at the pressure in the reservoir. With V and P of the gas in the tube known and effectively constant, it followed that the ideal gas law could be used to calculate the total number of moles of gas in the tube (n_{tube}) at a given time (t) and temperature (T). All the moles of gas exceeding n_{tube} were assumed to immediately exit the tube and stop reacting. In addition, following from the assumption that the chemical composition of the gas in the tube was homogeneous, the chemical composition of the gas exiting the tube would equal it. The gas swept into the GC/MS would

comprise the number of moles of each product eluted over the duration of the process.

Formulating governing equations for the envisioned/idealized process in terms of mole fractions (X_k),

$$X_k = \frac{n_k}{n_{tube}} = \frac{n_k RT}{PV} \tag{1}$$

where n_k is the number of moles of species k in the tube and R is the universal gas constant, we obtained for a system with K (total) species,

$$\frac{dX_k}{dt} = \frac{RT}{PV}\left[\dot{\omega}_k V - \left(X_k V \sum_{k=1}^{K} \dot{\omega}_k\right) - \left(X_k \frac{dT}{dt}\frac{PV}{RT^2}\right)\right] + \frac{X_k}{T}\left(\frac{dT}{dt}\right) \tag{2}$$

where $\dot{\omega}_k$ is the molar production rate of species k per unit volume due to chemical reactions. The term $\dot{\omega}_k V$ represents the (temporal) rate of change of n_k due to chemical reactions. The term $X_k V \sum_{k=1}^{K} \dot{\omega}_k$ represents the rate of n_k's elution from the tube driven by the rate at which moles of gas exceeding n_{tube} are being generated by the pyrolysis process. The term $X_k \frac{dT}{dt}\frac{PV}{RT^2}$ represents the rate of n_k's elution from the tube driven by changes in the gas's temperature. And the term $\frac{X_k}{T}\left(\frac{dT}{dt}\right)$ acts to normalize the X_k distribution such that $\sum_{k=1}^{K} X_k$ equals 1.

To facilitate the computation of thermodynamic properties and chemical kinetic parameters, the model was integrated into an in-house, precommercial version of SENKIN (Lutz et al. 1988; McQuaid 2020a). The system of equations was solved with a slightly modified version of DASPK (Li and Petzold 1999). The relative tolerance (RTOL) value was 1×10^{-8} and the absolute tolerance (ATOL) value was 1×10^{-13}.

With respect to specifying initial conditions, we noted that the starting temperature of the interface in which the pyroprobe was housed (175 °C) was higher than DTE's normal boiling point (170 °C). Moreover, distributed on quartz wool, it would have a high surface area–to–volume ratio. Therefore, we presumed based on previous experience in modeling condensed phase-to-gas-phase mass transfer processes (McQuaid et al. 2021) that the sample would be completely vaporized prior to the heating coil being energized.[*]

[*] To corroborate this presumption, we calculated the time it would take a 1-mg spherical droplet at its normal boiling point to completely evaporate and found it would be 20 ms. Since the sample's evaporation rate is proportional to its surface area, and a sphere represents the smallest surface area–to–volume ratio possible, 20 ms would represent an upper limit for the time it would take a sample to completely evaporate in the experiments if the attractive interaction between DTE and the quartz wool was negligible. That being said, the 20-s delay between the arrival of "headspace" DTE (peak 15) and DTE desorbed from the quartz wool (peak 18) is difficult to reconcile with this assumption. Thus, at this time we would not rule out the possibility that the interaction between liquid DTE and the quartz wool was non-negligible.

In addition, given the mass of the sample (m_{samp} = 1 mg), we found that the number of moles it comprised (7.3×10^{-6}) exceeded n_{tube} at 175 °C and 1.52 atm (5.1×10^{-6}). Moreover, because DTE is much heavier than He, we further assumed it would displace He as it evaporated, and thus that the starting chemical composition in the tube would be nearly pure DTE ($X_{DTE} \sim 1$), with the excess DTE (2.2×10^{-6} mol) immediately eluting from the tube without reacting. We refer to this quantity hereafter as $n_k^{t_0}$, where t_0 corresponds to the moment the heating coil was energized.

We computed the total number of moles of each species eluted from the tube while the heating coil was energized $\left(n_k^{t_0<t<t_f}\right)$ per

$$n_k^{t_0<t<t_f} = V \int_{t_0}^{t_f} X_k(t) \left[\left(\sum_{k=1}^{K} \dot{\omega}_k(t) \right) + \left(\frac{dT}{dt} \frac{P}{RT^2} \right) \right] dt \tag{3}$$

where t_f was the moment corresponding to the coil being deenergized. The equation was numerically integrated using the trapezoidal rule. To compute the total number of moles of each species that would be eluted to the GC/MS (n_k^f), $n_k^{t_0}$ and $n_k^{t_0<t<t_f}$ were added to the number of moles of each species in the tube at the end of the simulation ($n_k^{t_f}$),

$$n_k^{t_f} = X_k(t_f) \frac{RT}{PV} \tag{4}$$

yielding

$$n_k^f = n_k^{t_0} + n_k^{t_0<t<t_f} + n_k^{t_f}. \tag{5}$$

To verify that the numerical integration method was sufficiently accurate for the purposes of the study, we confirmed that the total mass of the products (m_{prod})

$$m_{prod} = \sum_{k=1}^{K} n_k^f MW_k \tag{6}$$

equaled m_{samp} to within ±0.001%. We also verified that $\sum_{k=1}^{K} X_k(t)$ was approximately 1 for all *t*.

3.2 Chemical Kinetics Mechanism

Details of the development of the chemical kinetics mechanism employed for this study are summarized elsewhere (Chen et al. 2023a). Briefly, quantum mechanics–based electronic structure methods (QM-ESMs) were employed to characterize minimum energy paths (MEPs) for ring-forming reactions with the potential to be important in DTE's pyrolysis. MEPs for six reaction types were characterized, and they were employed to parameterize formulae for computing the reactions' rate coefficients and the species' thermodynamic properties. Those formulae were combined with a mechanism built to model the pyrolysis and combustion of 6-

ethenyl-2,8,12,16-octadecetetraene (Chen et al. 2023b). Subsequently updated, a subset of that mechanism was employed for this study. It comprised formulae for computing rate coefficients for 1942 elementary reactions and thermodynamic properties for 774 species.

After running the four HR simulations using the (full) 1942 reaction-774 species mechanism, we eliminated all species (and reactions involving them) whose mole fractions did not exceed ATOL (1×10^{-13}) at any point in at least one of the simulations. Rerunning the four HR simulations with that mechanism, which comprised 1750 reactions and 687 species, we found that it produced n_k^f values that were within 1% of the respective value produced with the full mechanism. This mechanism is provided in an addendum to this report (Chen et al. 2024).

4. Results

4.1 Measured Abundances

To facilitate the comparison of measured and model-predicted results, the measurements provided in Table 1 of ARL-TN-1148 (Pesce-Rodriguez et al. 2023) were re-reduced. Our analysis included (1) eliminating from consideration all species that were attributed to processes other than the one of interest, (2) summing the (raw) total ion currents (IC_k) for the two chromatogram features attributed to DTE, and (3) converting the IC_k values into (relative) molar quantities (n_k^{GC}) by dividing them by an estimate for the species' total ionization cross section (Q_k) at 70 eV, namely,

$$n_k^{GC} \propto \frac{IC_k}{Q_k} \tag{7}$$

where the Q_k were estimated based on a group additivity method proposed by Fitch and Sauter (1983). Considerations underlying the decision to employ this approach to relating n_k^{GC} and IC_k are discussed in the Appendix.

Lacking information necessary to compute absolute molar quantities, we normalized the n_k^{GC} distributions at each T_{sp} so that they summed to 1, producing a set of parameters (a_k^{GC}) (referred to herein as "normalized abundances")

$$a_k^{GC}(T_{sp}) = c' \frac{n_k^{GC}(T_{sp})}{\sum_k^K n_k^{GC}(T_{sp})}, \tag{8}$$

where c' was a constant for scaling the distribution to facilitate comparisons to an analogous parameter derived from the modeling results.

Combined, there were 20 different species attributed to pyrolysis products observed in the four experiments. Table 1 provides their $a_k^{GC}(c' = 1)$ values along with

a_{DTE}^{GC}'s at each T_{sp}. For reference, the table also provides the Q_k values employed to compute them.

Table 1 GC/MS-based normalized abundances (a_k^{GC}): $c' = 1$

Compound	Q (Å^2)[a]	175 °C	500 °C	700 °C	1000 °C
propene	8.8	. . .	. . .	0.036	0.086
1,3-butadiene (1,3-BD)	10.2	. . .	0.056	0.160	0.175
1-pentene	14.5	. . .	. . .	0.013	0.027
1,3-cyclopentadiene (1,3-CPD)	11.6	. . .	. . .	0.016	0.027
1,5-hexadiene (1,5-HD)	16.0	. . .	0.024	0.144	0.115
benzene	13.0	. . .	. . .	0.016	0.103
1,3-cyclohexadiene (1,3-CHD)	14.5	. . .	. . .	0.028	. . .
1,5-heptadiene	18.9	. . .	. . .	0.005	. . .
tricyclo[2.2.1.0(2,6)]heptane	17.4	. . .	. . .	0.007	. . .
4-methylcyclohexene	18.9	. . .	. . .	0.004	. . .
toluene	15.9	. . .	. . .	. . .	0.029
3-methyl-1,3,5-hexatriene	17.4	. . .	. . .	0.003	. . .
1,3,5-cycloheptatriene	15.9	. . .	. . .	0.008	. . .
3-(2-propenyl)-1-cyclopentene	20.3	. . .	. . .	0.002	. . .
4-ethenyl-cyclohexene	20.3	. . .	. . .	0.002	. . .
styrene	17.4	. . .	. . .	. . .	0.013
1,5-cyclooctadiene	20.3	. . .	. . .	0.009	. . .
3-(2-propenyl)-cyclohexene	23.2	. . .	. . .	0.008	. . .
1,5,9-decatriene (DTE)[b]	26.1	1.000	0.919	0.541	0.405
1,3-butylienyl-benzene	21.7	. . .	. . .	. . .	0.006
naphthalene	20.2	. . .	. . .	. . .	0.015

[a] Estimate from the Fitch and Sauter model discussed in the Appendix
[b] Comprises both cis and trans conformers

4.2 Model-Predicted Abundances

4.2.1 175 °C

As reported previously (Pesce-Rodriguez et al. 2023), there was no evidence for the pyrolysis of DTE in the T_{sp} = 175 °C experiment.* The HR model's predictions for this experiment were consistent with this finding. However, its prediction for the evolution of the cis:trans DTE ratio warrants discussion.

As already noted, the NMR-based measurement of the sample employed in the experiments indicated it was 52% cis-DTE and 48% trans-DTE, and that ratio was employed to specify the gas's composition at t_0 in all simulations. A chemical equilibrium calculation performed with STANJAN (Reynolds 1986) indicated that at 175 °C and 1.52 atm, an equilibrium distribution of the two conformers would comprise 87% trans-DTE and 13% cis-DTE. However, the HR model predicted that there would be effectively no change from the starting ratio after 20 s at

* As discussed in Section 2.2, chromatogram features for seven organic compounds with relatively high molecular weights were observed but their source appeared to be something other than the process of interest.

175 °C. (Per the model, it would take ~2.5 min to effect a 0.1% change in either percentage.)

This finding could be rationalized because, as noted in Section 2.2, we found there to be a barrier of approximately 70 kcal/mol to the direct interconversion between the two (via rotation about the C=C bond) using high-level QM-ESMs. Indeed, the most energetically favorable path between cis-DTE and trans-DTE, per the QM-ESM calculations, involved a third species, namely, 4-vinyl-1,7-octatriene (VOD). VOD was the only other species in the mechanism whose mole fraction reached a numerically significant value over the course of the T_{sp}= 175 °C simulation. That being said, $Q_{VOD}n_{VOD}^{f}$ was only 1.6 × 10^{-8} mol-Å^2, and as (first) suggested by a result presented in Section 4.3.2 and corroborated by others discussed herein, we estimated that a species' $Q_k n_k^f$ value had to exceed 1 × 10^{-6} mol-Å^2 to be observed in a chromatogram. Thus, the lack of a feature attributable to VOD in the chromatogram was not considered cause for concern.

4.2.2 500 °C

As indicated in Table 1, the only pyrolysis products observed in the chromatogram produced by the T_{sp} = 500 °C experiment were 1,3-butadiene (1,3-BD) and 1,5-hexadiene (1,5-HD).

To compare the model-predicted n_k^f values to a_k^{GC} values, the n_k^f values were normalized to produce a distribution that summed to 1,

$$a_k^{pred}(T_{sp}) = \frac{n_k^f(T_{sp})}{\sum_k^K n_k^f(T_{sp})} \tag{9}$$

The value for c' in Eq. 8 was then chosen such that

$$a_{1,3-BD}^{pred}(T_{sp}) = a_{1,3-BD}^{GC}(T_{sp}). \tag{10}$$

This approach to comparing measured and model-predicted results was based on several considerations. Because our conceptualization of the experiment predicated that any moles of the starting DTE sample in excess of n_{tube} would elute from the tube prior to pyrolysis taking place, unlike the n_k^f predictions for all other species, the n_{DTE}^f predictions were a function of m_{samp}. However, m_{samp} was not actually measured and could have varied between experiments. Moreover, while we were interested in how well the model predicted the abundances of all species relative to one another, given (1) our inability to (reliably) derive from IC_k values the absolute concentrations of the species and (2) the huge difference between IC_{DTE} and the IC_k for all other species, we prioritized comparing the model's predictions for the relative abundances of the pyrolysis products, which favored a scaling based on the results for one of them.

The decision to scale $a_k^{GC}(T_{sp})$ based on results for 1,3-BD followed from several observations. For one, $IC_{1,3-BD}$ and $n_{1,3-BD}^{t_f}$ had significant values at all conditions of interest. In addition, unlike IC_{DTE}, there was little doubt that $IC_{1,3-BD}$ was well below saturation levels in all the experiments. Lastly, $Q_{1,3-BD}$ was (seemingly) well established, and (we thought) would promulgate the least amount of analytical uncertainty deriving from uncertainty in this parameter.

Figure 3 compares the $a_k^{pred}(500)$ and $a_k^{GC}(500)$ values for the 21 species that were detected in at least one D/P-GC/MS experiment. The value of c' employed to scale the $a_k^{GC}(500)$ distribution was 1.20. Also shown are $a_k^{pred}(500)$ values for methane and ethylene. Neither was observed in the chromatogram of any experiment, but the model predicted they would be produced in significant quantities in all $T_{sp} \geq 500$ °C experiments. The model also predicted that $a_{H_2}^{pred}(500)$ would be comparable to $a_{ethylene}^{pred}(500)$. However, H_2's molecular weight is similar to He's and its concentration was much lower than He's. Therefore, IC_{H_2} was not measurable, obviating it as a basis for validating the model. Thus, no attempt to assess $a_{H_2}^{pred}(T_{sp})$ values was made.

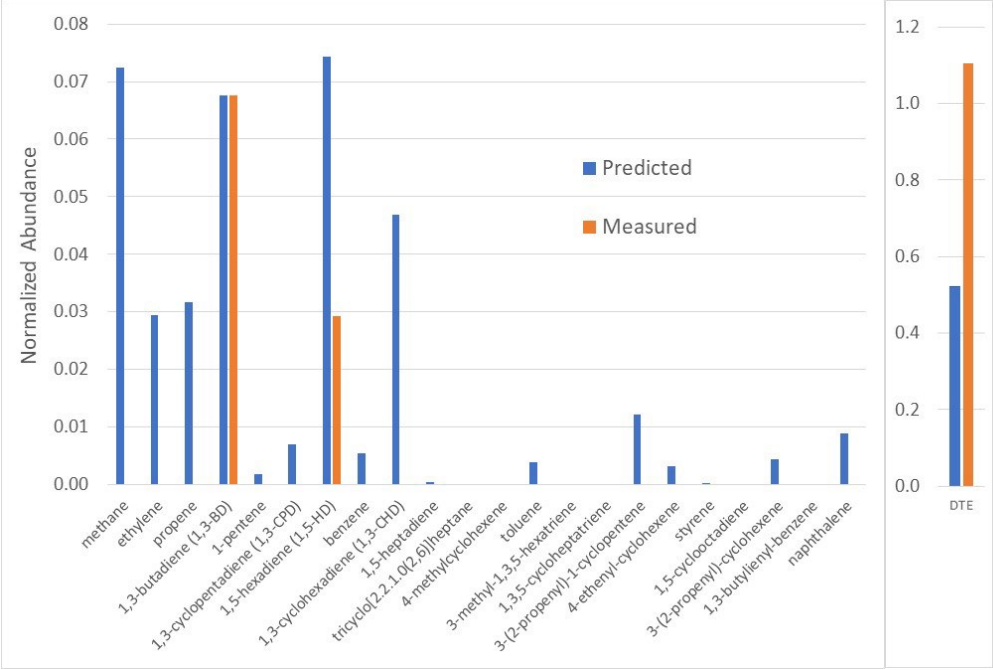

Fig. 3 Normalized abundances: T_{sp} = 500 °C

As Fig. 3 shows, the model predicted that 1,3-BD and 1,5-HD would have two of the three highest (molar) abundances, which was encouraging. (Methane's abundance fell between those two.) However, there were a fair number of notable discrepancies.

Prominent was a_{DTE}^{pred} being considerably lower than a_{DTE}^{GC}. However, we could think of several reasons why that might be. For one, the mass of the sample in the experiment had the potential to be greater than 1 mg. It also seemed possible that Q_{DTE} (relative to $Q_{1,3-BD}$) was underpredicted. Saturation of the detector, the impact of which is discussed in more detail in Section 4.3.2, would have biased the results in the opposite direction and was found in every other case considered. But overall, we saw no reason to be overly concerned about this result.

Of more concern were the a_k^{pred} values for methane, ethylene, propene, and 1,3-CHD. Although comparable to $a_{1,3-BD}^{pred}$ and $a_{1,5-HD}^{pred}$, features attributable to these species were not observed in the chromatogram. Subsequently computing their $Q_k n_k^f$ values, we found that all exceeded the 1×10^{-6} mol-Å^2 threshold we came to believe represented a prediction that a species would be observed in a chromatogram. (See Table 2.) Indeed, screening the remainder of the $Q_k n_k^f$ values on that basis, we found five other species that the model predicted would be observed but were not. A hypothesis that at least partially reconciles these observations is introduced and discussed in Section 4.3.1.

In addition to those findings, we observed that there were 2.5×10^{-6} more moles of gas at the end of the process than there were at its beginning. Given that only 5.1×10^{-6} mol of gas were subject to pyrolysis, they represented an approximately 50% increase. The sum of the n_k^f values for the 23 species listed in Fig. 3 plus $n_{H_2}^f$ accounted for 91% of the total. Of the remaining 751 species in the mechanism, the only ones with $Q_k n_k^f$ values greater than 1×10^{-6} mol-Å^2 are listed in Table 2.

Table 2 $Q_k n_k^f$ values for selected species: T_{sp} = 500 °C[a]

Compound	$Q_k n_k^f$ (mol-Å^2/10^{-6})
methane	3.1
ethylene	1.7
propene	2.7
1,3-BD	6.7
1,5-HD	11.6
1,3-CHD	6.7
3-(2-propenyl)-1-cyclopentene	2.4
3-(2-propenyl)-cyclohexene	1.0
naphthalene	1.8
4-vinylcyclopentene	2.1
VOD	6.6

[a] Except for 1,3-BD and 1,5-HD, the species listed in this table comprise all those in the simulation that had a $Q_k n_k^f$ value greater than 1×10^{-6} mol-Å^2 but was not observed in the chromatogram.

4.2.3 700 °C

In the T_{sp} = 700 °C experiment, 16 species attributable to DTE's pyrolysis were observed. As in the T_{sp} = 500 °C experiment, 1,3-BD's and 1,5-HD's $a_k^{GC}(700)$ values were the largest. The $a_k^{GC}(700)$ values for the remainder of the species were approximately 1/10th (or less) as large.

Figure 4 compares $a_k^{pred}(700)$ and $a_k^{GC}(700)$ values for methane, ethylene, and all species that were detected in at least one D/P–GC/MS experiment. Overall, the agreement was better than it was in the T_{sp} = 500 °C case. Compared to a_k^{GC} values, the magnitudes of $a_{propene}^{pred}$, $a_{1,3-BD}^{pred}$, $a_{1,3-CPD}^{pred}$, $a_{1,5-HD}^{pred}$, $a_{benzene}^{pred}$, and $a_{1,3-CHD}^{pred}$ relative to each other were very encouraging.

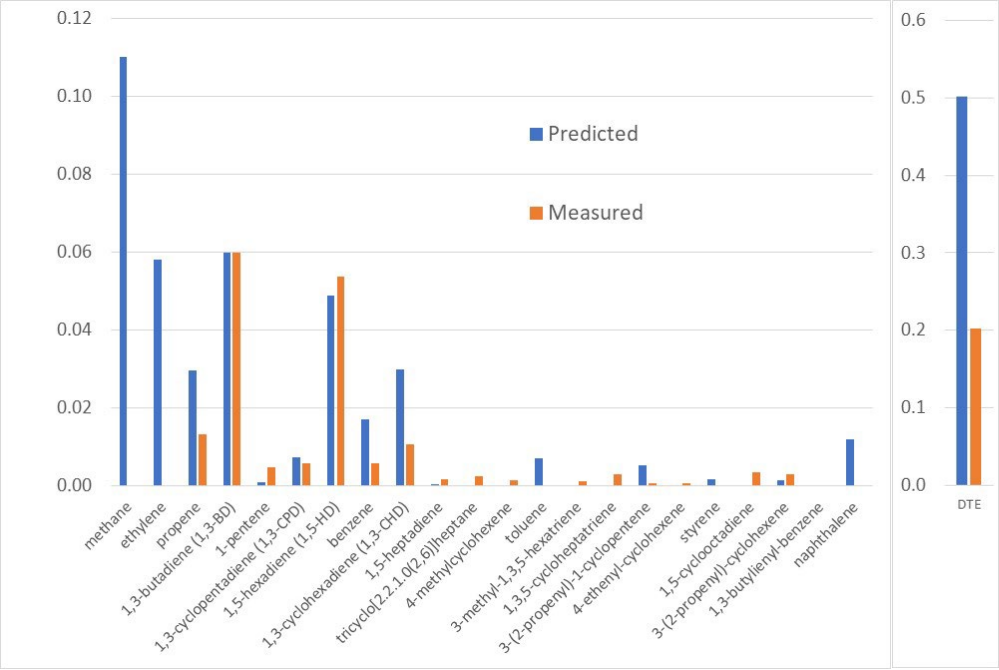

Fig. 4 Normalized abundances: T_{sp} = 700 °C

The difference between a_{DTE}^{GC} and a_{DTE}^{pred} was not encouraging but could be rationalized. Briefly, the relationship between n_k^{GC} and IC_k expressed in Eq. 7 will become nonlinear for n_k^{GC} values that approach a level that will saturate the detector. More specifically, IC_k will underrepresent the n_k^{GC} values of such species relative to the n_k^{GC} for species that are well below that level. Given that the chromatogram feature attributable to DTE flattened out in all the experiments, we believe it quite likely that DTE's concentration produced IC_k values that were near the saturation limit. Thus, we were inclined to disregard the discrepancies. (Had a_{DTE}^{GC} values been greater than a_{DTE}^{pred}, there would have been cause for concern.)

Given the reasonable agreement between $a_k^{pred}(700)$ and $a_k^{GC}(700)$ values for the pyrolysis products, we believed they provided a basis for estimating the GC/MS's

detection threshold. For example, the $a_{1,3-CPD}^{pred}$ and $a_{1,3-CPD}^{GC}$ values were very similar and $IC_{1,3-CPD}$ was at the low end of the detectable range. Since $n_{1,3-CPD}^{f}$ was 7.6 × 10^{-8} mol and $Q_{1,3-CPD}$ was 11.6 Å^2, $n_{1,3-CPD}^{f} Q_{1,3-CPD}$ was 8.8 × 10^{-7} mol-Å^2, implying that species with $Q_k n_k^f$ values greater than 1 × 10^{-6} mol-Å^2 should be detected.

That threshold was subsequently corroborated when coupled with a hypothesis as to why the model was overpredicting the abundances of methane, ethylene, and other species. (That hypothesis is introduced in Section 4.3.1.) Therefore, it was the threshold above which values were taken to represent a prediction that a species would be observed in a chromatogram.

Table 3 lists species that were not observed in the chromatogram but whose $Q_k n_k^f$ values exceeded 1 × 10^{-6} mol-Å^2. In addition to methane and ethylene, the $Q_k n_k^f$ values for naphthalene, VOD, and indene were well above this value. As in the T_{sp} = 500 °C case, the lack of evidence for VOD in the chromatogram could be rationalized.

Table 3 $Q_k n_k^f$ values for selected species: T_{sp} = 700 °C[a]

Compound	$Q_k n_k^f$ (mol-Å^2/10^{-6})
methane	5.0
ethylene	3.5
1,3-BD	6.3
1,5-HD	8.0
toluene	1.2
naphthalene	2.5
4-vinylcyclopentene	1.2
VOD	7.1
indene	2.6

[a] Except for 1,3-BD and 1,5-HD, the species listed in this table comprise all those in the simulation that had a $Q_k n_k^f$ value greater than 1 × 10^{-6} mol-Å^2 but was not observed in the chromatogram.

We observed that there were 3.0 × 10^{-6} more moles in the system at the end of the process than at its beginning. That increase was 20% greater than the increase predicted for the T_{sp} = 500 °C simulation. The sum of the n_k^f values for the 23 species listed in Fig. 4 plus $n_{H_2}^f$ accounted for 91% of the total.

4.2.4 1000 °C

As indicated in Table 1, there were fewer pyrolysis products observed in the T_{sp} = 1000 °C experiment (10) than there were in the T_{sp} = 700 °C experiment (16). Eight of the larger nonaromatic compounds observed in the 700 °C experiment were not

observed, and four aromatic compounds that were not observed in the 700 °C experiment were (i.e., toluene, styrene, 1,3-butylienylbenzene, and naphthalene). 1,3-BD and 1,5-HD again had the highest a_k^{GC} values.

Figure 5 compares $a_k^{pred}(1000)$ and $a_{DTE}^{GC}(c' = 0.32)$ values for methane, ethylene, and all species that were detected in at least one D/P-GC/MS experiment. Overall, the agreement was comparable to that observed in the T_{sp} = 700 °C case. Compared to a_k^{GC} values, the magnitudes of $a_{propene}^{pred}$, $a_{1,3-BD}^{pred}$, $a_{1,3-CPD}^{pred}$, $a_{1,5-HD}^{pred}$, and $a_{benzene}^{pred}$ relative to each other were reasonable. In addition, the model predicted detectable quantities of aromatic compounds that were not detected in the T_{sp} < 1000 °C experiments (i.e., toluene, styrene, and naphthalene). However, as shown in Table 4, the model (again) predicted that the process would produce detectable quantities of methane and ethylene along with five other species (besides VOD), but they were not observed in the chromatogram.

In addition to these findings, we observed that the simulated system comprised 1.07×10^{-5} mol at the end of the process, 3.4×10^{-6} mol more than at its start. This increase was approximately 10% greater than the increase predicted for the T_{sp} = 700 °C experiment. The sum of n_k^f for species whose a_k^{pred} values are shown in Fig. 5 plus $n_{H_2}^f$ accounted for 92% of the total.

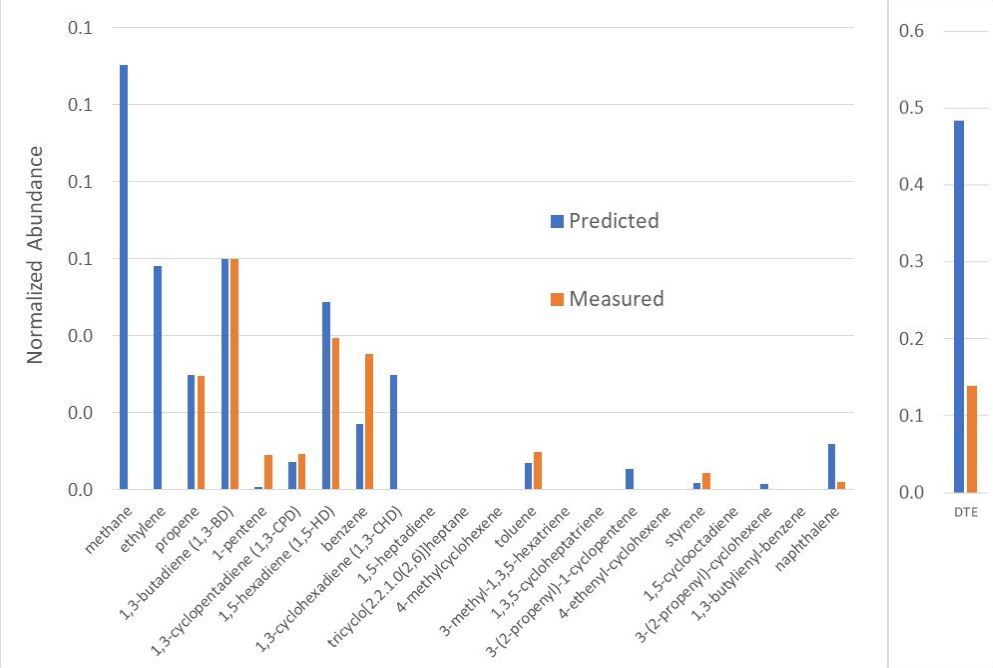

Fig. 5 Normalized abundances: T_{sp} = 1000 °C

Table 4 $Q_k n_k^f$ **values for selected species:** T_{sp} **= 1000 °C**[a]

Compound	$Q_k n_k^f$ (mol-Å^2/10^{-6})
methane	5.3
ethylene	1.9
1,3-BD	6.1
1,5-HD	8.5
1,3-CHD	3.4
3-(2-propenyl)-1-cyclopentene	1.1
4-vinylcyclopentene	1.3
VOD	7.1
indene	2.4
fluoranthene	1.5

[a] Except for 1,3-BD and 1,5-HD, the species listed in this table comprise all those in the simulation that had a $Q_k n_k^f$ value greater than 1 × 10^{-6} mol-Å^2 but were not observed in the chromatogram.

4.2.5 Initial Thoughts on Discrepancies between Measured and Predicted Abundances for Methane and Ethylene

To us, the most puzzling discrepancies between a_k^{GC} and a_k^{pred} values were those for methane and ethylene. Considering whether the mechanism might be deficient, we performed a sensitivity analysis and found that many of the most important reactions for the creation of methane and ethylene involved ring-containing molecules that were imported from AramcoMech 3.0 (Zhou et al. 2018) and had rate coefficient formulae that we believed require further evaluation.

That being said, Vermeire et al. (2017) pyrolyzed 1,5-HD diluted in He in a jet-stirred reactor and observed methane and ethylene (as well as H_2) to be the dominant products of processes at conditions that, except for the level of dilution in He, were similar to those in our experiments. (The conditions in their experiments were 1 atm, temperatures from 527 to 777 °C, and a residence time of 2 s.) Given also that 1,5-HD is effectively a substructure of DTE (see Fig. 6) and was both observed and predicted to be a major product of DTE's pyrolysis in this study, we believed methane and ethylene had the potential to form at detectable levels. Thus, we did not think the discrepancies were due solely to the mechanism, and other explanations were sought.

DTE 1,5-HD

Fig. 6 The molecular structures of DTE and 1,5-HD

4.3 Pyroprobe-Induced Pyrolysis Dynamics

Concluding that the model's predictions for the end states of the pyroprobe-induced pyrolysis of DTE had some merit, we thought its predictions for the temporal dynamics of the processes warranted consideration. In the subsections that follow, we present results from the T_{sp} = 500, 700, and 1000 °C simulations. (Results from the T_{sp} = 175 °C simulation are not presented because pyrolysis was not predicted or observed in the experiment.)

4.3.1 500 °C

As discussed in Section 4.2.2, $a_{1,5-HD}^{pred}(500)$ and $a_{1,3-BD}^{pred}(500)$ were significantly larger relative to $a_{DTE}^{pred}(500)$ than $a_{1,5-HD}^{GC}(500)$ and $a_{1,3-BD}^{GC}(500)$ were to $a_{DTE}^{GC}(500)$. The model also predicted that detectable quantities of methane, ethylene, and seven other organic compounds would be produced, but none were observed. The quantity of H_2 predicted was also non-negligible but as already mentioned was not measurable. Therefore, predictions for it could not be validated.

Figure 7 presents the temporal evolutions of the $X_{cis-DTE}$ and $X_{trans-DTE}$ predictions. As shown, they declined significantly prior to T_{sp} being reached, and they were effectively zero within about 2 s of the coil being energized.

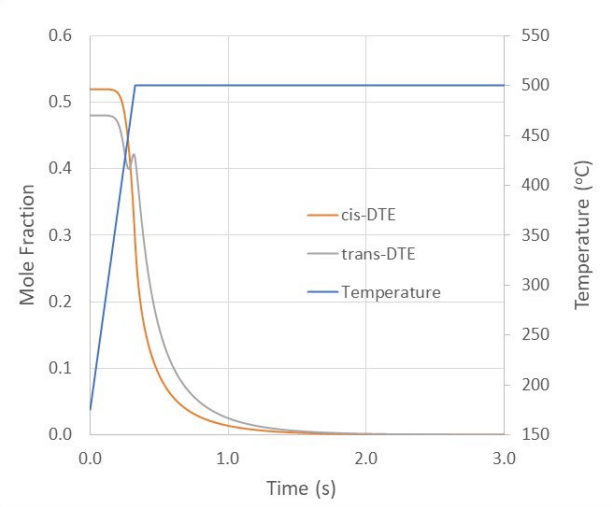

Fig. 7 Temporal evolutions of $X_{cis-DTE}$ and $X_{trans-DTE}$: T_{sp} = 500 °C

Figure 8 shows the temporal evolutions of the X_k of the six pyrolysis products with the largest a_k^{pred} values. All began to increase significantly at about 0.3 s and rose steadily thereafter until about 1.5 s. The $X_{1,5-HD}$ and $X_{1,3-BD}$ values then steadily declined while the X_k values for the smaller molecules increased or stayed about the same. (The trends observed for $t > 2$ s persisted for the remainder of the simulation's 20-s duration.)

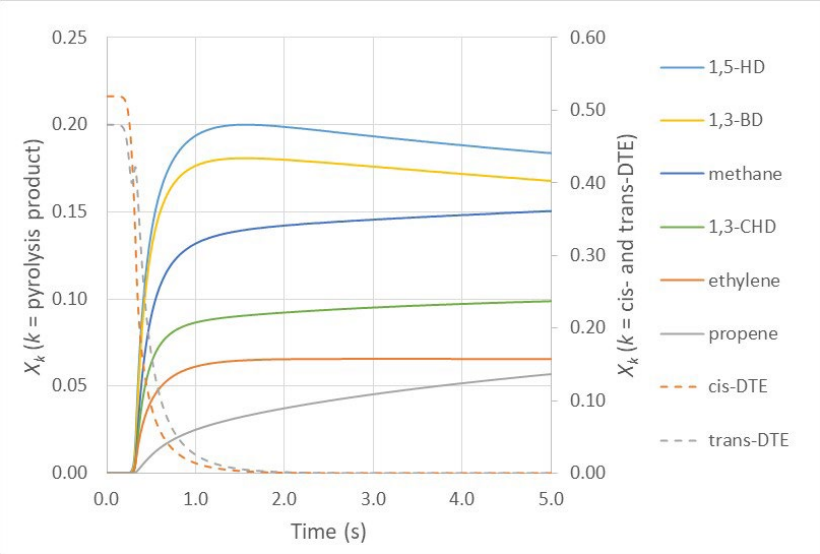

Fig. 8 Temporal evolutions of major (predicted) pyrolysis product X_k values: T_{sp} = 500 °C

Figure 9 shows the total molar elution rate and the separate contributions to that rate due to (1) chemical reactions and (2) the increase in the tube gas's temperature from t_0 to 0.325 s. Though the instantaneous change in the temperature ramp rate at 0.325 s was not physically realistic, we saw no need to provide a representation that was more so. (It would have been speculative, and it was considered unlikely that it would have altered the general conclusions that were drawn from the simulations.) From t_0 until about 0.24 s, the total rate was driven almost exclusively by the increase in temperature, which reduced n_{tube}. The gas eluted from the tube during this interval comprised primarily cis-DTE and trans-DTE.

At about 0.24 s, chemical reactivity began to make a noticeable contribution to the total elution rate, driving out unreacted cis- and trans-DTE (Fig. 9). As shown in Fig. 8, the chemical composition of the mixture continued to change while the heating coil was energized. However, as Fig. 9 shows, the model predicted that there was effectively no net increase in the total number of moles eluted from the tube after about 2.5 s, and (not shown) this remained the case for the 20-s duration of the simulation.

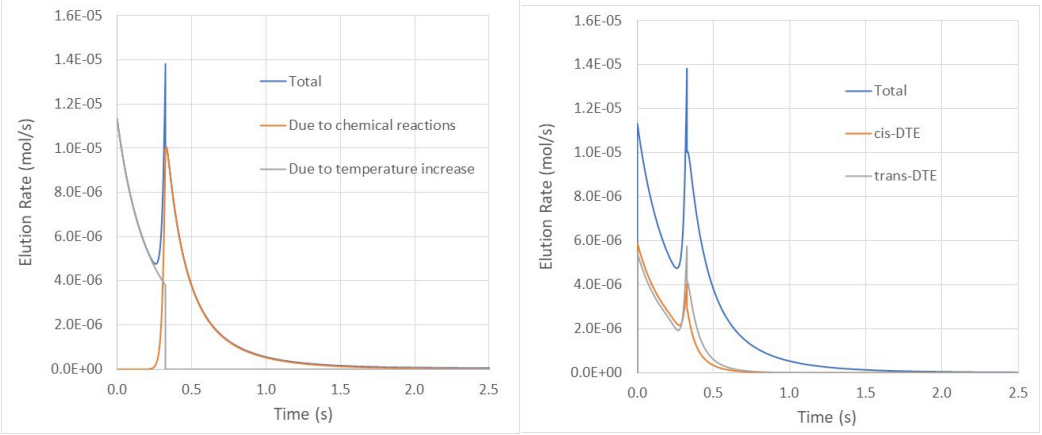

Fig. 9 Molar elution rate predictions for the T_{sp} = 500 °C experiment: total, cis-DTE, and trans-DTE

Figure 10 shows the molar elution rates for the six pyrolysis products with the largest a_k^{pred} values. Consistent with the results shown in Fig. 9, these predictions indicated that most of the pyrolysis products that eluted from the tube while the heating coil was energized (from t_0 to 20 s) did so very early in the heating cycle.

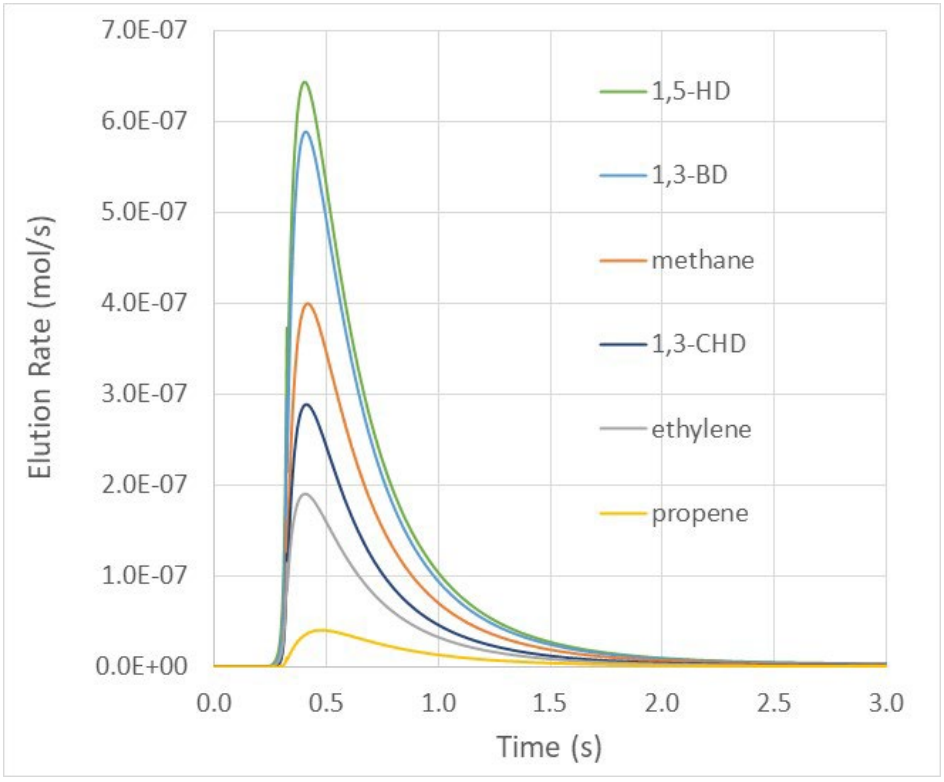

Fig. 10 Molar elution rate predictions for the T_{sp} = 500 °C experiment: pyrolysis products with the largest a_k^{pred} values

Table 5 compares the $n_k^{t_0<t<t_f}$ and $n_k^{t_f}$ values for the six pyrolysis products with the largest a_k^{pred} values. In each case, well over half of n_k^f was attributable to $n_k^{t_f}$. Searching for an explanation for the lack of chromatogram features attributable to methane, ethylene, propene, and 1,3-CHD, we noted that in each of these cases, the $n_k^{t_f}$ values were a larger fraction of n_k^f than they were in the cases of 1,3-BD and 1,5-HD. This prompted us to wonder whether the gas in the tube at the end of the coil's energization might be trapped in it, and thus not contribute to n_k^f (as assumed in Eq. 5).

Table 5 $n_k^{t_0<t<t_f}$ **and** $n_k^{t_f}$ **values for selected pyrolysis products:** T_{sp} **= 500 °C**

Compound	$n_k^{t_0<t<t_f}$	$n_k^{t_f}$	$n_k^{t_f}/n_k^f$
methane	2.0×10^{-7}	5.1×10^{-7}	0.72
ethylene	9.4×10^{-8}	1.9×10^{-7}	0.67
propene	3.6×10^{-8}	2.7×10^{-7}	0.88
1,3-BD	2.8×10^{-7}	3.9×10^{-7}	0.59
1,5-HD	3.0×10^{-7}	4.3×10^{-7}	0.59
1,3-CHD	1.4×10^{-7}	3.2×10^{-7}	0.70

Regarding this hypothesis, we note (first) that at the end of the (20-s) heating cycle, the model predicts the gas in the tube has approached an equilibrium thermochemical state. That is, there is effectively no net change in the number of moles of gas being produced by chemical reactions. (The term $\sum_{k=1}^{K} \dot{\omega}_k(t)$ in Eq. 3 is effectively zero.) In addition, as soon as the heating coil is deenergized, the gas in the tube will begin to cool. Though we have not attempted to model that part of the process, it is clear that the $\left(\frac{dT}{dt}\frac{P}{RT^2}\right)$ term in Eq. 3, which is positive while the heating coil raises the temperature from 175 °C to T_{sp} and drives gas from the tube, will be negative. Thus, rather than promoting the elution of gases from the tube, this term would promote the flow of He into the tube, hindering the pyrolysis products' escape.

To quantify the potential impact of $n_k^{t_f}$ not contributing to n_k^f, we computed "modified" normalized abundances per

$$n_k^{f'} = n_k^{t_0} + n_k^{t_0<t<t_f} \tag{11}$$

$$a_k^{pred'}(T_{sp}) = \frac{n_k^{f'}(T_{sp})}{\sum_k^K n_k^{f'}(T_{sp})} \tag{12}$$

and specified c' in Eq. 8 such that

$$a_{1,3-BD}^{pred'}(T_{sp}) = a_{1,3-BD}^{GC}(T_{sp}). \tag{13}$$

The value of c' necessary to achieve the equality was 0.71. The predictions are compared to the chromatogram-based values in Fig. 11. As shown, the agreement between $a_{DTE}^{pred'}$ and a_{DTE}^{GC} (c' = 0.71) was far better than the agreement between a_{DTE}^{pred} and a_{DTE}^{GC} (c' = 1.20) (see Fig. 3). Moreover, though not negligible, the $a_k^{pred'}$ values for methane, ethylene, propene, and 1,3-CHD were lower than their a_k^{pred} counterpart.

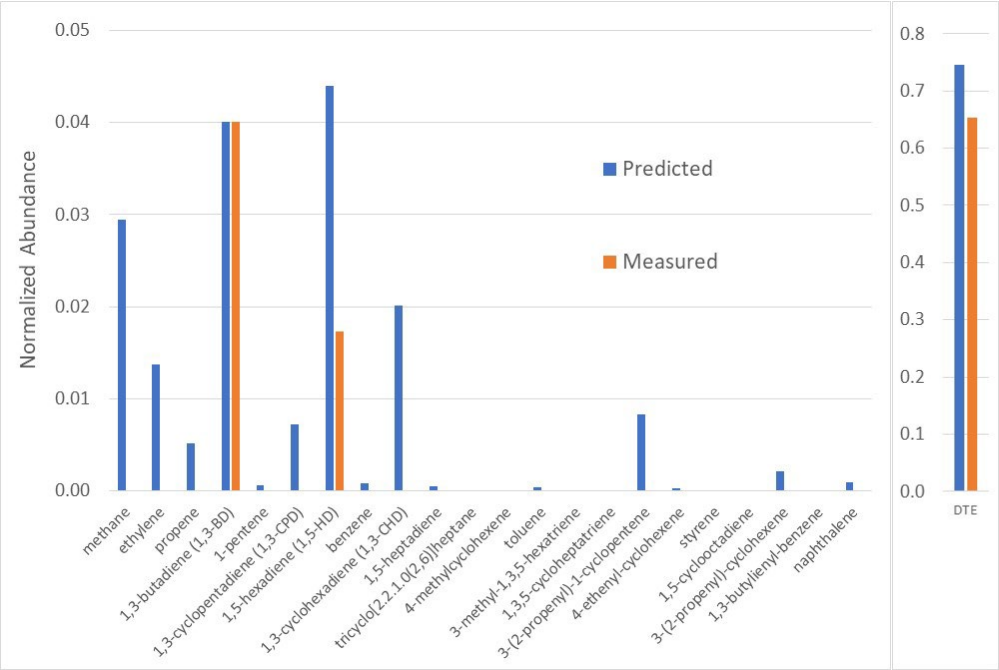

Fig. 11 Modified normalized abundances: T_{sp} = 500 °C

As for their detectability, Table 6 presents $Q_k n_k^{f'}$ for all the species (listed in Table 2) that had $Q_k n_k^f$ values greater than 1×10^{-6} mol-Å^2 but were not observed in the chromatogram. ($Q_k n_k^f$ values for 1,3-BD and 1,5-HD are shown for comparison.) It was observed that only 1,3-CHD and VOD had $Q_k n_k^{f'}$ values significantly greater than 1×10^{-6} mol-Å^2. Given that $n_k^{f'}$ was less than or equal to n_k^f for all species, by themselves the fact that $Q_k n_k^{f'}$ values were lower than their respective $Q_k n_k^f$ value might not have been noteworthy. However, the $Q_k n_k^{f'}$ values for 1,3-BD and 1,5-HD were still significantly higher than the (presumed) detection threshold, indicating that the hypothesis underlying this approach to analyzing the simulation's results did not over-correct them while at the same time reducing all but 1,3-CHD's and VOD's $Q_k n_k^{f'}$ values to the detection threshold or less. In addition, the discrepancy between $a_{DTE}^{pred'}(500)$ and $a_{DTE}^{GC}(500)$ was considerably less than the discrepancy between $a_{DTE}^{pred}(500)$ and $a_{DTE}^{GC}(500)$ and it exhibited the bias $[a_{DTE}^{pred'}(500) < a_{DTE}^{GC}(500)]$ we expected based on our suspicion that n_{DTE} values were at levels approaching those that would saturate the detector.

Table 6 $Q_k n_k^{f'}$ **values for selected species:** T_{sp} **= 500 °C**[a]

Compound	$Q_k n_k^{f'}$ (mol-Å^2/10^{-6})
methane	0.9
ethylene	0.6
propene	0.3
1,3-BD	2.8
1,5-HD	4.8
1,3-CHD	2.0
3-(2-propenyl)-1-cyclopentene	1.1
3-(2-propenyl)-cyclohexene	0.3
naphthalene	0.1
4-vinylcyclopentene	1.1
VOD	6.6

[a] Except for 1,3-BD and 1,5-HD, the species listed in this table comprise all those in the simulation that had a $Q_k n_k^f$ (not $Q_k n_k^{f'}$) value greater than 1 × 10^{-6} mol-Å^2 but was not observed in the chromatogram.

4.3.2 700 °C

As discussed in Section 4.2.3, we were encouraged by the overall agreement between $\{a_k^{pred}\}$ and $\{a_k^{GC}\}$ values. However, the model (again) predicted that methane and ethylene would be produced in detectable quantities, but they were not observed in the chromatogram.

Figure 12 shows the temporal evolutions of $X_{cis-DTE}$ and $X_{trans-DTE}$ (in the tube). As shown, the model predicted that they would be effectively zero less than 0.5 s after the coil was energized, and therefore prior to the gas reaching 700 °C (at 0.525 s).

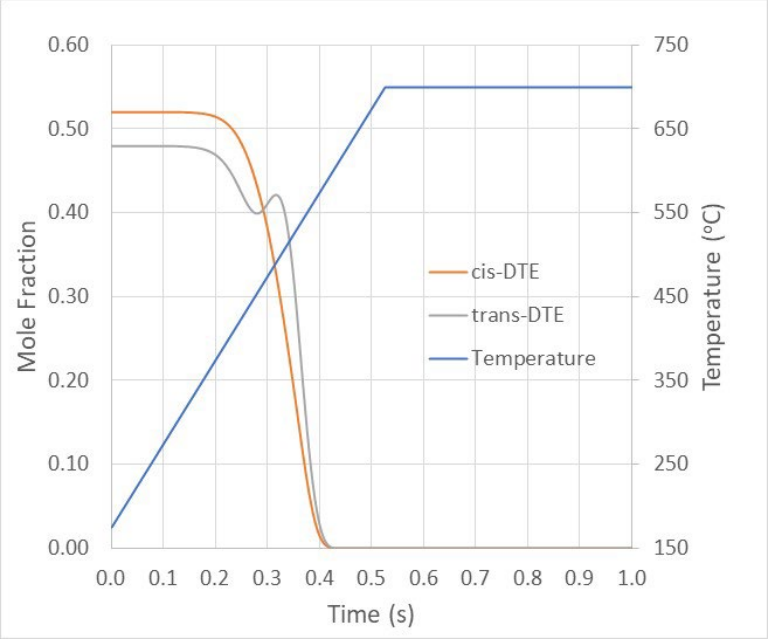

Fig. 12 **Temporal evolutions of** $X_{cis-DTE}$ **and** $X_{trans-DTE}$**:** T_{sp} **= 700 °C**

Figure 13 shows the temporal evolutions of the X_k of the six pyrolysis products with the largest a_k^{pred} values. As in the T_{sp} = 500 °C simulation, all rose steadily from their first significant increase at about 0.3 s. However, in this simulation, $X_{1,5-HD}$ and $X_{1,3-BD}$ peaked at approximately 0.42 s, and the former declined to zero in less than 2 s. $X_{1,3-BD}$ declined less precipitously. Not shown, the trends observed in the X_k values for t > 2 s continued for the 20-s duration of the simulation.

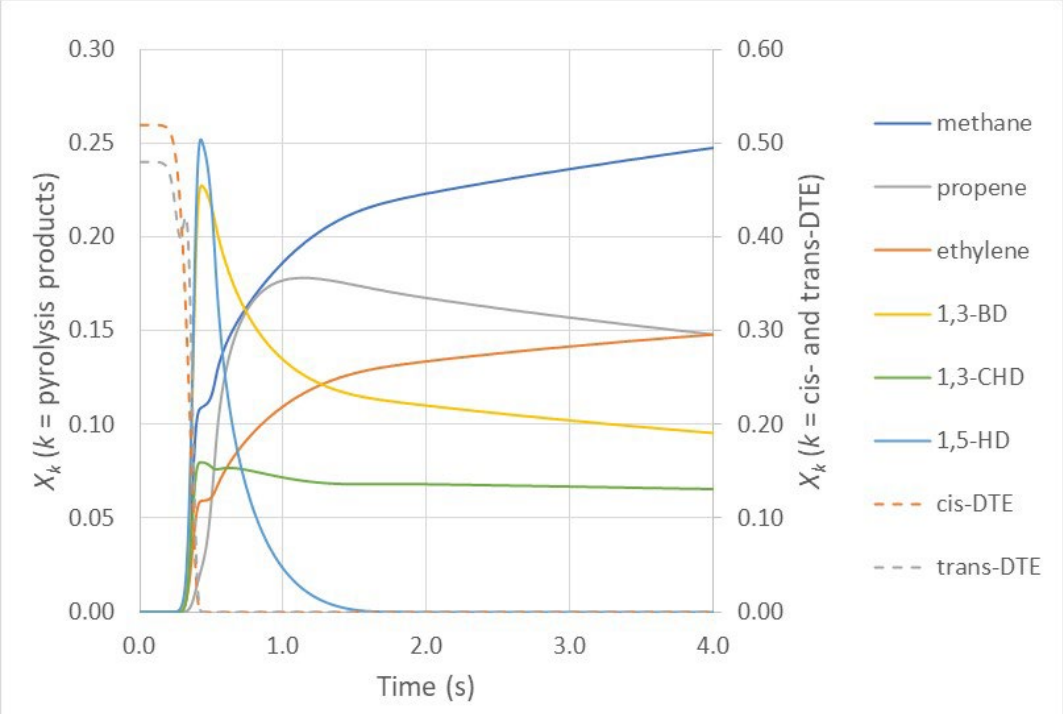

Fig. 13 Temporal evolutions of major (predicted) pyrolysis product X_k values: T_{sp}= 700 °C

Figure 14 shows the total molar elution rate and the contributions to it driven by chemical reactions and the increase in tube gas's temperature from t_0 to the moment T_{sp} was reached (at 0.525 s). Again, the abrupt change in the contribution due to the temperature increase caused by the model's representation for the gas's temperature profile was not physically realistic, but we saw no need to address this issue. Identical to the T_{sp} = 500 °C simulation, from t_0 until about 0.24 s, the total rate was driven almost exclusively by the increase in temperature. Thereafter, chemical reactivity made a noticeable contribution. Unlike the T_{sp} = 500 °C simulation, the first spike in the total elution rate was followed by a second spike that onset at about 0.44 s. As shown in Fig. 13, the chemical composition of the mixture continued to change after this spike. But as shown in Fig. 14, there was effectively no net increase in the total number of eluted moles after about 1.5 s. Although not shown, this continued to be the case for the remainder of the simulation's 20-s duration.

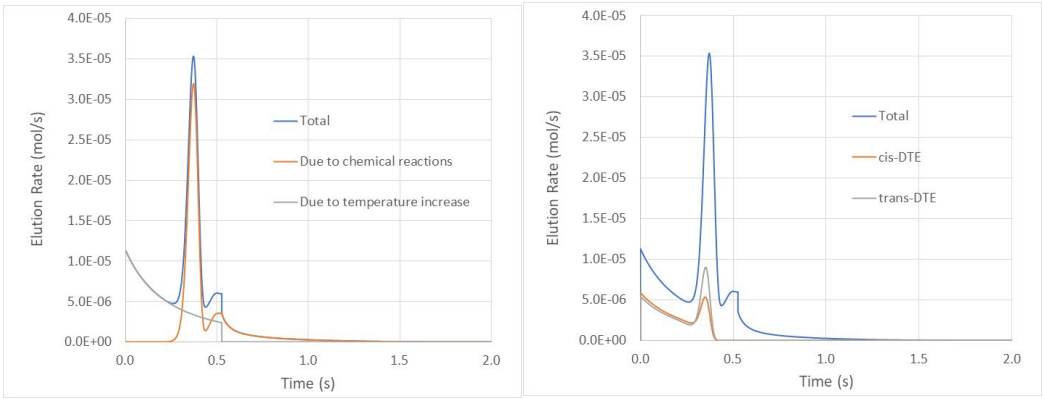

Fig. 14 Molar elution rate predictions for the T_{sp} = 700 °C experiment: total, cis-DTE, and trans-DTE

Figure 15 shows the molar elution rates for the six pyrolysis products with the largest a_k^{pred} values. Coupled with consideration of Fig. 14, it shows that production of these species was largely responsible for the second spike in the total molar elution rate, and the $n_k^{t_0<t<t_f}$ values for these species were largely attributable to their production and elution from the tube within 1 s of the coil being energized. We also note that the ordering of these species' elution rates during the first elution rate spike was the same as it was in the T_{sp} = 500 °C simulation. The ordering of the species' elution rates during the second rate spike was also essentially the same except for propene's. Its elution rate increased more rapidly than the others.

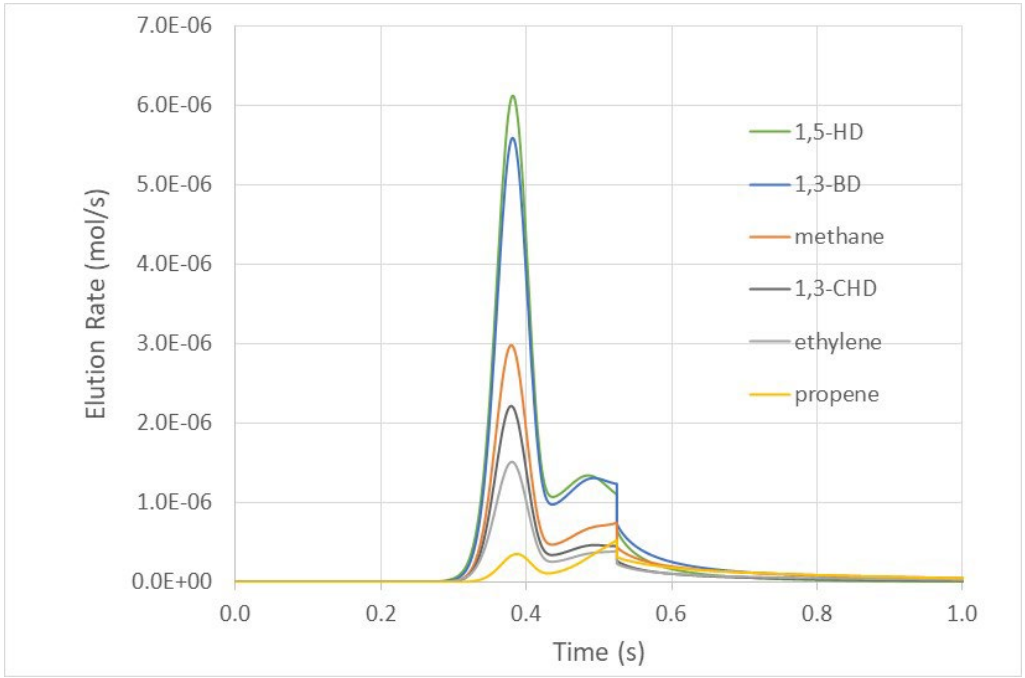

Fig. 15 Molar elution rate predictions for the T_{sp} = 700 °C experiment: pyrolysis products with the largest a_k^{pred} values

Figure 16 shows the molar elution rates for 6 of the other 12 GC/MS-identified pyrolysis products. (The maximum rates of the other six were lower than those shown.) The rates for the species shown in Fig. 16 are notable mainly for exhibiting the same temporal behavior as those for the six species with the largest a_k^{pred} values.

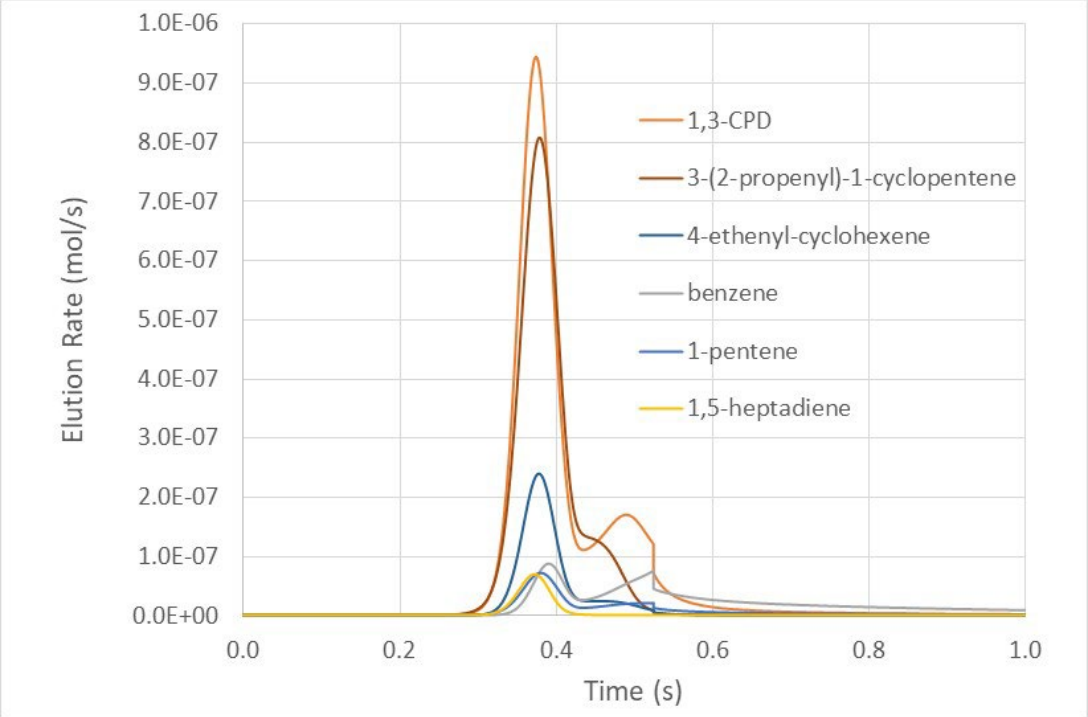

Fig. 16 Molar elution rate predictions for the T_{sp} = 700 °C experiment: other pyrolysis products

Table 7 compares the $n_k^{t_0<t<t_f}$ and $n_k^{t_f}$ values for methane, ethylene, and the four most prominent chromatogram-identified pyrolysis products. Similar to the analogous analysis of results produced by the T_{sp} = 500 °C simulation, the $n_k^{t_f}$ values for methane, ethylene, and propene were more than half of their respective n_k^f value. However, the contributions of $n_k^{t_f}$ values to n_k^f values for 1,3-BD, 1,5-HD, and 1,3-CHD were even lower than those found in the T_{sp} = 500 °C simulation. Only 18% of $n_{1,3-BD}^f$ was attributable to $n_{1,3-BD}^{t_f}$, and (effectively) none of $n_{1,5-HD}^f$ was attributable to $n_{1,5-HD}^{t_f}$.

Table 7 $n_k^{t_0<t<t_f}$ **and** $n_k^{t_f}$ **values for selected pyrolysis products:** T_{sp} **= 700 °C**

Compound	$n_k^{t_0<t<t_f}$	$n_k^{t_f}$	$n_k^{t_f}/n_k^f$
methane	3.3×10^{-7}	8.1×10^{-6}	0.71
ethylene	1.8×10^{-8}	4.2×10^{-7}	0.71
propene	1.3×10^{-8}	1.8×10^{-7}	0.59
1,3-BD	5.1×10^{-7}	1.1×10^{-7}	0.18
1,5-HD	5.0×10^{-7}	7.0×10^{-11}	0.00
1,3-CHD	1.4×10^{-7}	1.1×10^{-7}	0.34

To further quantify the potential impact of the hypothesis that $n_k^{t_f}$ did not (fully) contribute to n_k^f, $a_k^{pred'}(700)$ values were computed and are compared to $a_k^{GC}(700)$ (c' = 0.40) values in Fig. 17. Compared to the $a_k^{pred}(700)$ vs. a_k^{GC} (c' = 0.37) case presented in Fig. 4, the agreement between $a_{DTE}^{pred'}(700)$ and a_{DTE}^{GC} (c' = 0.40) was slightly worse. The agreement between $a_k^{pred'}(700)$ and a_k^{GC} (c' = 0.40) for all other species besides methane and ethylene was the same. The $a_k^{pred'}$ values for methane and ethylene were significantly less than their respective a_k^{pred} value.

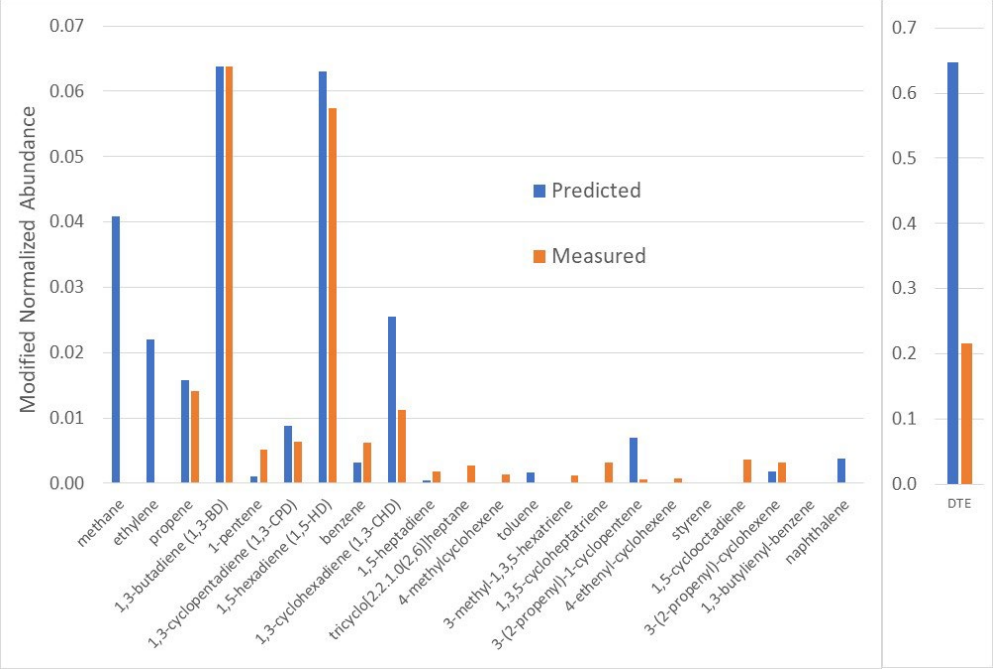

Fig. 17 Modified normalized abundances: T_{sp} **= 700 °C**

Table 8 presents the $n_k^{f'}$ predictions for all species in the T_{sp} = 700 °C simulation whose $Q_k n_k^f$ value was greater than 1×10^{-6} mol-Å^2 but were not observed in the chromatogram. Although the $Q_k n_k^{f'}$ values for methane and ethylene were at or near the threshold, we believed that the uncertainties underlying the conversion of IC_k values into n_k per Eq. 7 could be as high a factor of two. Thus, $Q_k n_k^{f'}$

predictions that were half as large as those calculated were not unthinkable and would be well below the detection threshold. As such, we believed the results corroborated the hypothesis that the gas in the tube at the end of the heating cycle may have been trapped.

Table 8 $Q_k n_k^{f'}$ **values for selected species:** T_{sp} **= 700 °C**[a]

Compound	$Q_k n_k^{f'}$ (mol-Å^2/10^{-6})
methane	1.4
ethylene	1.0
1,3-BD	5.2
1,5-HD	8.0
toluene	0.2
naphthalene	0.6
4-vinylcyclopentene	1.2
VOD	7.1
indene	0.4

[a] Except for 1,3-BD and 1,5-HD, the species listed in this table comprise all those in the simulation that had a $Q_k n_k^f$ value greater than 1×10^{-6} mol-Å^2 but was not observed in the chromatogram.

Likewise, the $Q_k n_k^{f'}$ values for the three aromatic compounds in the table (i.e., toluene, naphthalene, and indene), which were not observed in the chromatogram, were also below the detection threshold, further supporting our hypothesis.

4.3.3 1000 °C

As discussed in Section 4.2.4, the overall agreement between $\{a_k^{pred}(1000)\}$ and $\{a_k^{GC}(1000)\}$ was encouraging. However, the model (again) predicted that on a molar basis, methane would be the largest single contributor to the total, but it was not observed in the chromatogram. Ethylene, which had the sixth largest $a_k^{pred}(1000)$ value, was also not observed.

Figure 18 shows the temporal evolutions of the mole fractions of cis- and trans-DTE (in the tube) and six of the seven pyrolysis products with the largest a_k^{pred} values. (The seventh was benzene, the results for which are discussed with results for other aromatic compounds.) The temporal evolutions of the mole fractions of cis- and trans-DTE were identical to those in the T_{sp} = 700 °C simulation. (Based on the T_{sp} = 700 °C simulation, this result was to be expected. The temperature ramp rates in the T_{sp} = 700 °C and T_{sp} = 1000 °C simulations were the same, and as shown in Fig. 12, there was no DTE in the tube by the time the temperature had reached 700 °C.) Like the 700 °C simulation, $X_{1,3-BD}$ and $X_{1,5-HD}$ values peaked at approximately 0.45 s. But in this case, they both declined to near zero within 1 s.

By 1 s, the mixture in the tube comprised almost exclusively methane, ethylene, and hydrogen, with $X_{ethylene}$ declining and X_{H_2} increasing thereafter.

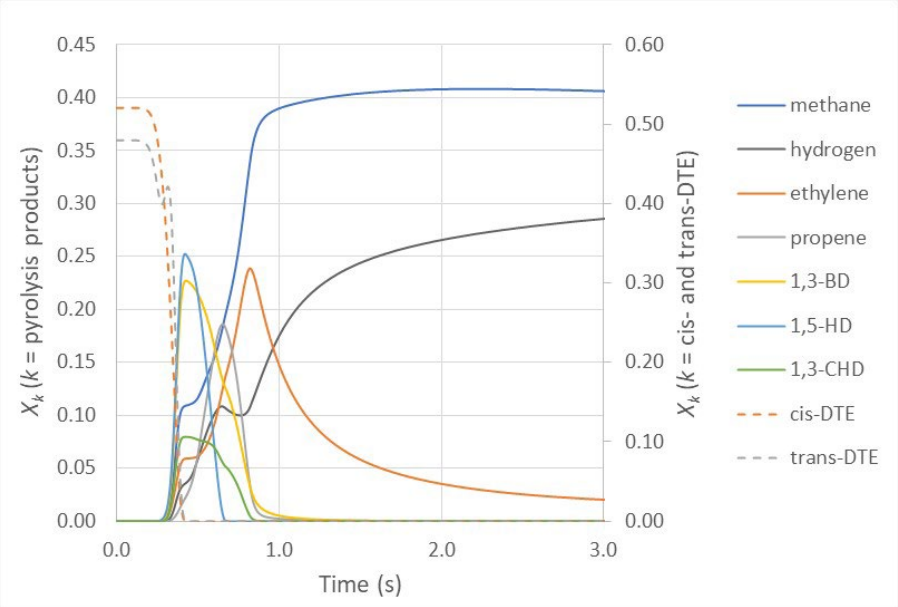

Fig. 18 Temporal evolutions of major (predicted) pyrolysis product X_k values: T_{sp} = 1000 °C

Figure 19 shows the total molar elution rate and the contributions to it driven by chemical reactions and the increase in the tube gas's temperature from t_0 to 0.825 s when T_{sp} was reached. Again, the abrupt change in the rate at 0.825 s was not physically realistic but considered ignorable. The process from t_0 to 0.525 s was identical to that in the T_{sp} = 700 °C simulation. After 0.525 s, the second increase in the total elution rate that onset at about 0.44 s plateaued out to about 0.62 s before steeply declining. This feature was followed by a third spike that reached a maximum at about 0.8 s. There was essentially no change in $\sum n_k^{t_0<t<t_f}$ after about 1.25 s.

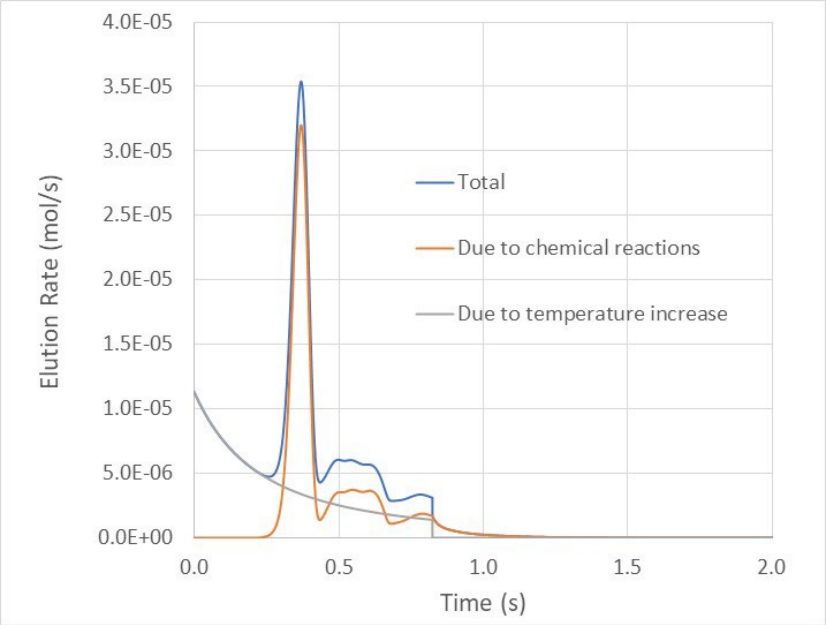

Fig. 19 Molar elution rate predictions for the T_{sp} = 1000 °C experiment

Figure 20 shows the molar elution rates for the six pyrolysis products with the highest $\{a_k^{pred}\}$ values. For the three largest molecules in this set (1,5-HD, 1,3-BD, and 1,3-CHD), the decline in their molar elution rates that started just prior to the temperature reaching 700 °C (at 0.525 s) continued until they bottomed near zero at 0.9 s and they did not increase thereafter. Propene's rate of elution continued to increase from its value at 0.525 s out to about 0.62 s, then declined thereafter. Methane's and ethylene's elution rates were oscillatory, but generally increased until T_{sp} was reached. They then declined to zero by about 1.2 s.

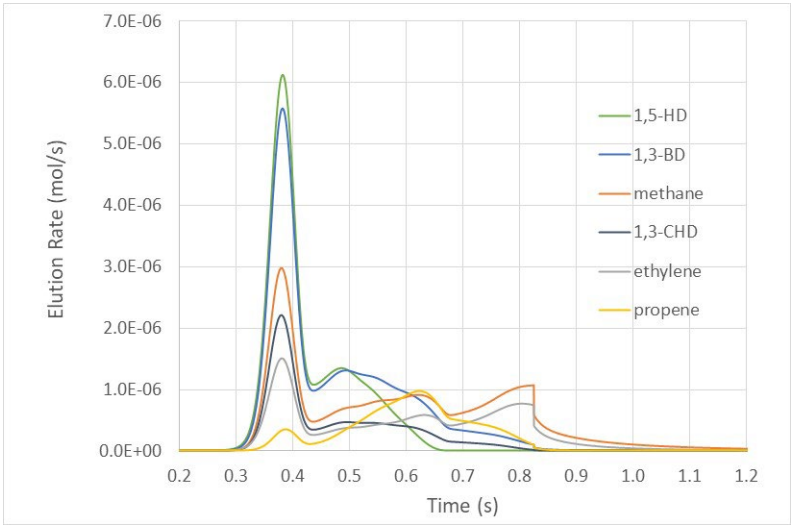

Fig. 20 Molar elution rate predictions for the T_{sp} = 1000 °C experiment: pyrolysis products with the largest a_k^{pred} values

Figure 21 shows the molar elution rates for five of the other six pyrolysis products observed in the chromatogram produced by the T_{sp} = 1000 °C experiment. (The elution rate predictions for 1,3-butylienylbenzene, which was the only other pyrolysis product observed in the chromatogram, were effectively zero for all t.) The only nonaromatic compound of the five was 1-pentene. It, along with the aromatic compounds, contributed to the second spike in the total elution rate. The aromatics with methane and ethylene contributed to the third elution rate spike. Except for methane and ethylene, no nonaromatic compound did.

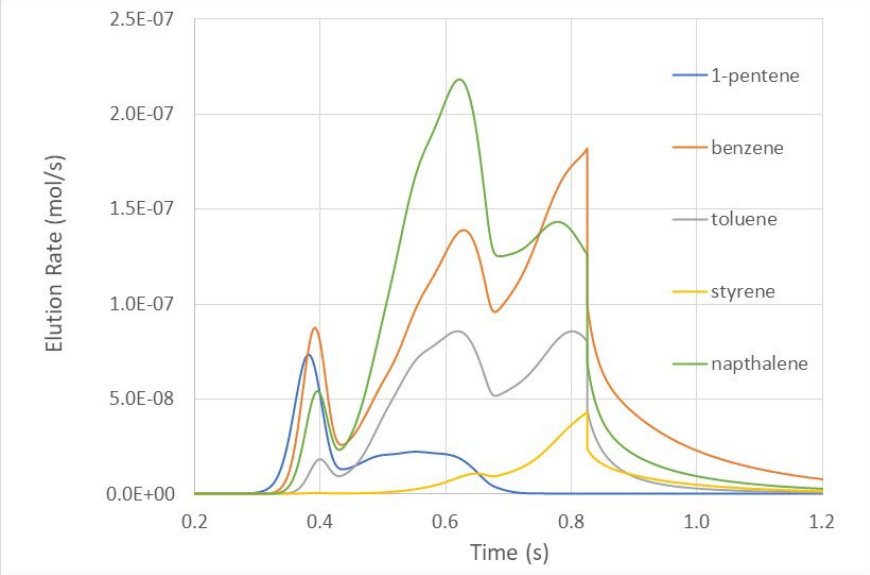

Fig. 21 Molar elution rate predictions for the T_{sp} = 1000 °C experiment: aromatic compounds and 1-pentene

Table 9 compares the $n_k^{t_0<t<t_f}$ and $n_k^{t_f}$ values for methane, ethylene, the four most prominent pyrolysis products, and the four aromatic compounds that were observed in the chromatogram. Consistent with our hypothesis that the contents in the tube at the end of the coil's energization might be trapped, the $n_k^{t_f}$ values for methane, ethylene, and propene were over half of n_k^f while none of $n_{1,3-BD}^f$ or $n_{1,5-HD}^f$ was attributable to the corresponding $n_k^{t_f}$.

Table 9 $n_k^{t_0<t<t_f}$ **and** $n_k^{t_f}$ **values for selected pyrolysis products:** T_{sp} **= 1000 °C**

Compound	$n_k^{t_0<t<t_f}$	$n_k^{t_f}$	$n_k^{t_f}/n_k^f$
methane	5.6×10^{-7}	6.3×10^{-6}	0.53
ethylene	3.1×10^{-8}	1.8×10^{-8}	0.06
propene	2.2×10^{-8}	2.0×10^{-10}	0.00
1,3-BD	6.0×10^{-7}	0.0	0.00
1,5-HD	5.3×10^{-7}	0.0	0.00
1,3-CHD	2.3×10^{-7}	0.0	0.00
benzene	7.3×10^{-8}	3.3×10^{-7}	0.88
toluene	2.8×10^{-8}	1.3×10^{-8}	0.31
styrene	7.5×10^{-9}	6.9×10^{-9}	0.48
naphthalene	6.3×10^{-8}	2.7×10^{-9}	0.41

To quantify the potential impact of the hypothesis, $a_k^{pred'}(1000)$ values were computed and are compared to $a_k^{GC}(1000)$ values in Fig. 22. As found for T_{sp} = 700 °C, the $a_{methane}^{pred'}(1000)$ and $a_{ethylene}^{pred'}(1000)$ values were smaller, but not insignificant. In addition, for three of the four aromatic compounds (benzene, toluene, and styrene) there was worse agreement between $a_k^{pred'}(1000)$ and $a_k^{GC}(1000)$ values than between $a_k^{pred}(1000)$ and $a_k^{GC}(1000)$ values. (In these cases, both $\{a_k^{pred}(1000)\}$ and $\{a_k^{pred'}(1000)\}$ values were low relative to $\{a_k^{GC}(1000)\}$; the $\{a_k^{pred'}(1000)\}$ values were lower.) Nonetheless, to the extent we suspect that Eq. 11 overestimates the degree to which pyrolysis products are trapped in the tube, when coupled with the results presented in Fig. 5, we were not dissatisfied with the agreement.

Table 10 presents the $n_k^{f'}$ predictions for all species in the T_{sp} = 1000 °C simulation whose $Q_k n_k^f$ value was greater than 1×10^{-6} mol-Å^2 but were not observed in the chromatogram. As found for the T_{sp} = 700 °C simulation discussed in Section 4.3.2, the $Q_k n_k^{f'}$ values for methane and ethylene were above the threshold. However, given the uncertainties underlying the conversion of IC_k values into n_k per Eq. 7, $Q_k n_k^{f'}$ predictions that are half as large as those calculated were not unthinkable and would be at or below the detection threshold.

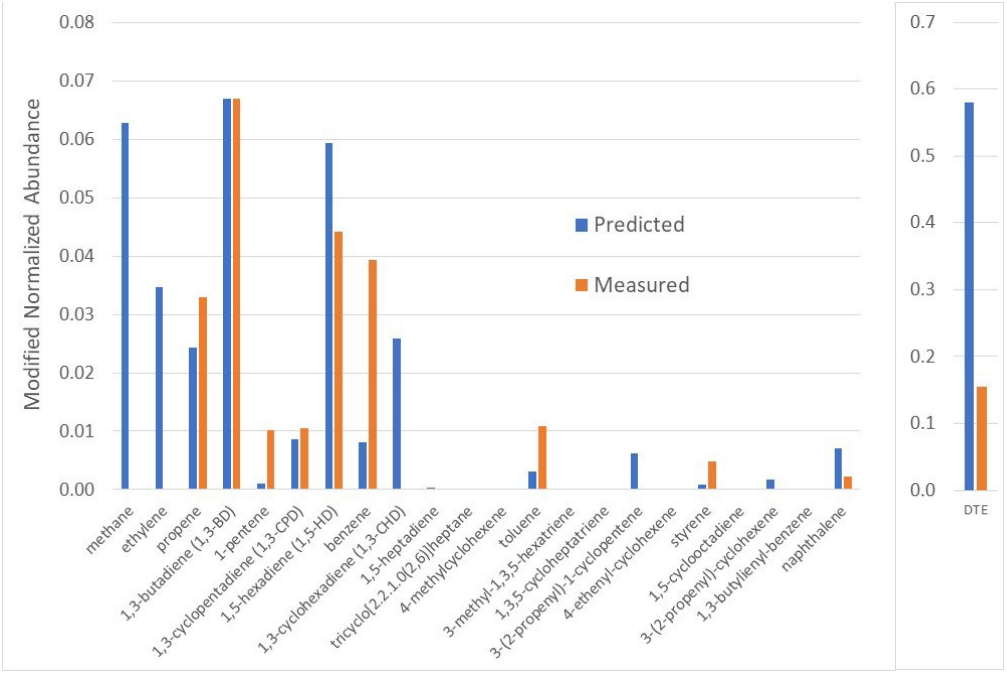

Fig. 22 Modified normalized abundances: T_{sp} = 1000 °C

Table 10 $Q_k n_k^{f'}$ values for selected species: T_{sp} = 1000 °C[a]

Compound	$Q_k n_k^{f'}$ (mol-Å^2/10^{-6})
methane	2.5
ethylene	1.8
1,3-BD	6.1
1,5-HD	8.5
1,3-CHD	3.4
3-(2-propenyl)-1-cyclopentene	1.1
4-vinylcyclopentene	1.3
VOD	7.1
indene	1.2
fluoranthene	0.5

[a] Except for 1,3-BD and 1,5-HD, the species listed in this table comprise all those in the simulation that had a $Q_k n_k^f$ value greater than 1×10^{-6} mol-Å^2 but were not observed in the chromatogram.

4.3.4 Heat Release Rate

Having extensively employed variously defined measures of "heat release rate" ($\dot{q}$) as bases for producing skeletal mechanisms for use in computational fluid dynamics models of deflagration scenarios, we plan to use them as bases for ML model training. However, we were not sure whether they would be convenient and appropriate bases for ranking the importance of reactions for pyrolysis scenarios. To obtain a preliminary answer to that question, we computed a $\dot{q}$ per

$$\dot{q} = V \sum_k^K \dot{\omega}_k h_k \tag{13}$$

where h_k is the enthalpy per mole of species k.

The predictions produced by the T_{sp} = 1000 °C simulation are shown in Fig. 23. It was observed that the changes in $\dot{q}$ corresponded to changes in the total elution rates shown in Fig. 19 (as one would expect). The first spike in $\dot{q}$ corresponded to the first spike in the total elution rate and was positive, indicating the process (as a whole) in this interval was endothermic. Following a second (small) endothermic spike, the ensuing values were negative, indicating the process was exothermic thereafter. Finding these results interesting, but not particularly relevant to our program's objectives, we will analyze them further if time and resources permit.

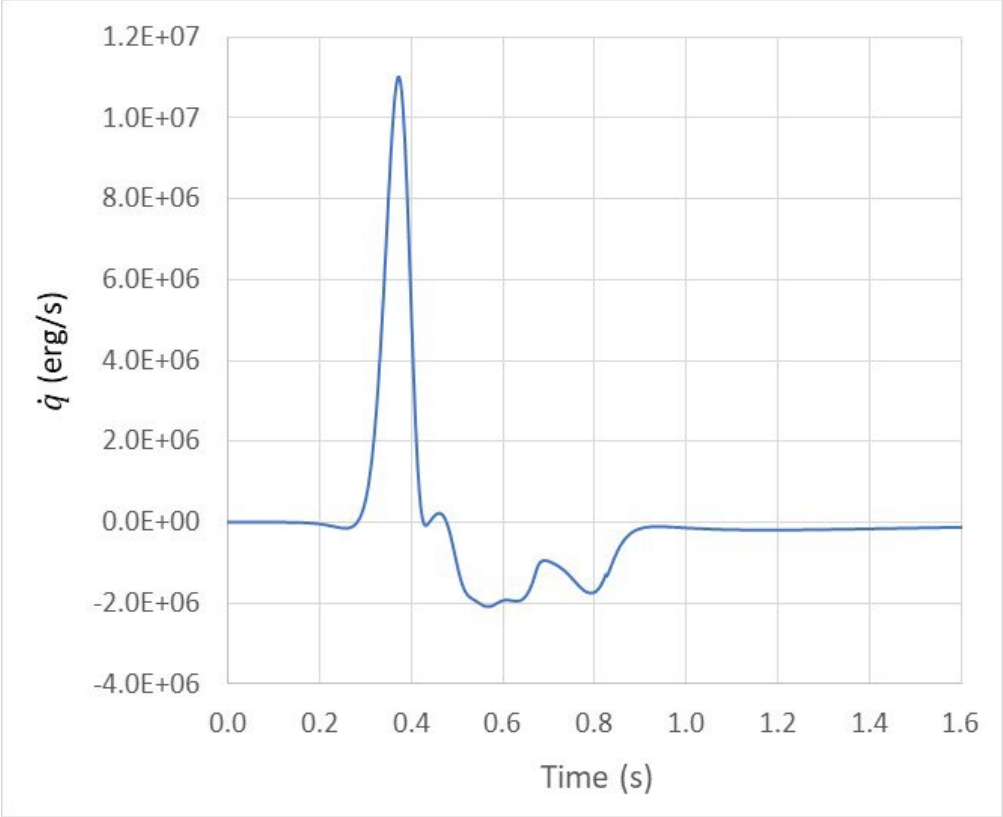

Fig. 23 Predicted $\dot{q}(t)$: T_{sp} = 1000 °C

5. Future Work: ML Model Training

Based on the comparisons presented in the previous section, we concluded that the mechanism–model combination offers a representation of the D/P–GC/MS experiment that is sufficient to proceed to the next phase of our program to create ML-based models for reducing the time and cost necessary to create detailed finite-rate chemical kinetics mechanisms. In that phase, MIT's Reaction Mechanism Generator (RMG) will be employed to generate (what we hope is) a comprehensive

list of elementary reactions with non-negligible potentials to be important in the pyrolysis of DTE under the conditions of such experiments. For those that are not already in the mechanism, ML-based methods will be employed to rank their potential to be important. For those that are predicted to be important, high-level QM-ESMs will be employed to generate data needed to parameterize their rate coefficients and the thermodynamic properties of any species that are not already in the mechanism. Those formulae will be added to the existing mechanism, and their impact on the results assessed.

The bases we plan to employ to train ML models for ranking (or classifying) the relative importance of the reactions generated by RMG derive from our experience in formulating and applying the trial mechanism method (TMM) for mechanism reduction (Kotlar 2010; McQuaid 2013a; McQuaid 2020b). In the TMM, selected results of solutions to a set of canonical combustion problems produced by a "full" mechanism and trial mechanisms created by recursively eliminating reactions (one at a time) are compared. The magnitudes of differences in the results they produce are the basis for determining whether a reaction is important or not (for the application of interest).

To date, we have only employed the TMM to produce skeletal mechanisms for representing the combustion chemistry associated with deflagration scenarios. For such scenarios, we have found that results derived from solutions to closed-system, adiabatic HR problems (Kotlar 2010; McQuaid 2013a) and opposed-flow diffusion flame (OFDF) problems (McQuaid 2020b) are convenient and appropriate bases for that purpose. When employing solutions to HR problems, parameters whose values have been compared include the magnitudes of (local) maxima in (variations of) heat release rate ($\dot{q}_{max}$), the times at which those maxima occur ($t_{\dot{q}_{max}}$), and the final temperature (T_f). When employing solutions to OFDF problems, we have compared predictions for the temperature gradient at the fuel inlet ($dT/dx|_{x=0}$), the maximum temperature (T_{max}), and the location at which T_{max} occurs ($d_{T_{max}}$).

The HR model discussed herein is fundamentally different from those cases in several important respects. For one, it represents an open (vs. closed) system, and we were uncertain if there would be any ramifications related to that difference. More importantly, the temperature is specified (rather than predicted). Therefore, deviations in parameters analogous to T_f, $dT/dx|_{x=0}$, T_{max}, and $d_{T_{max}}$ cannot serve as bases for ranking a reaction's importance. In addition, because the process of interest was pyrolysis rather than combustion, it was not clear to us at the start of this investigation whether deviations in the values of parameters analogous to $\dot{q}_{max}$ and $t_{\dot{q}_{max}}$ would be convenient and appropriate bases for training.

The results presented in the previous section addressed these concerns. Indeed, they suggested numerous parameters for whom values produced by a full and a trial

mechanism could be compared to classify and/or rank a reaction's importance. For example, as indicated in Fig. 18, maxima in $X_{1,3-BD}(t)$ and $X_{1,5-HD}(t)$ plots and the times at which those maxima occur are possibilities. However, as discussed by McQuaid (2013b), there are advantages to using global rather than species-specific parameters. Therefore, we will employ (at least to start) deviations in the maxima in the total elution rate due to chemical reactions, the time at which those maxima occur, and $\sum n_k^f$ (or $\sum n_k^{f'}$). Other possibilities are $\dot{q}_{max}$ and $t_{\dot{q}_{max}}$. But given the similarities between the plots of total elution rate due to chemical reactions and $\dot{q}$, such comparisons may prove to be redundant.

As a first test of the efficacy of this approach, we will employ RMG to generate a mechanism for DTE, then employ ML-based models to rank the relative importance of reactions that are not in the current mechanism. For the highest ranked candidates, formulae for computing their rate coefficients will be derived from MEP results produced by high-level QM-ESMs. Those formulae will be added to the mechanism, and we will re-perform the simulations presented herein. Our hope/expectation is that the overall agreement between measured and predicted results will improve.

6. Conclusions

As part of a program to develop and apply ML methods with the potential to significantly reduce the time and cost needed to create detailed finite-rate chemical kinetics mechanisms, we formulated an HR model to simulate pyroprobe-induced pyrolysis. To evaluate the model, it was employed to simulate the pyrolysis of DTE that was realized in a set of D/P–GC/MS experiments whose results were previously reported. We found that it reasonably reproduced the measurement-derived concentrations of pyrolysis products relative to one another and as a function of T_{sp} if in addition to the general suppositions made in formulating the model, we made the following three assumptions:

- The ion currents produced by the DTE concentrations generated in the experiments approached saturation limits and therefore underrepresented those concentrations relative to the concentrations of the pyrolysis products.
- The pyrolysis products in the tube at the end of the heating cycle did not elute to the GC/MS (on a relevant time scale).
- The threshold for the detection of individual species was approximately 1×10^{-6} mol-Å^2.

The first author (at least) considers all of them plausible (to some degree). The threshold above which the relationship between a species concentration and the ion

current it produces becomes nonlinear could perhaps be established experimentally. The latter two hypotheses address the puzzling discrepancy between the model's predictions for the molar quantities of methane and ethylene that would be produced in the experiments and the lack of evidence for them in the chromatograms.

In addition to obtaining predictions for the relative concentrations of pyrolysis products at the end of the process, we produced and analyzed model predictions for the temporal evolutions of various parameters. The results were extremely interesting, suggesting behavior that could not have been surmised from the GC/MS results alone. For one, the model predicted that during the 20-s heating cycle, most of the products that were swept to the GC/MS were formed within 3 s of the heating coil being energized. Driven at first simply by thermal expansion as the temperature increased from its starting value (175 °C) to T_{sp}, the elution rate steadily declined until an increase in the moles of gas due to chemical reactions began to make a significant contribution at about 0.26 s (435 °C). In the T_{sp} = 500 °C simulation, chemical reactivity was essentially the sole driver of elution until a quasi-equilibrium was reached about 3 s after the coil's energization started. In the T_{sp} = 700 °C simulation, the temperature increased through this first chemically driven spike and initiated a second one. In the T_{sp} = 1000 °C simulation, the temperature increased through the first two chemically driven spikes and initiated a third. Such results suggest that the model could be helpful in formulating D/P-GC/MS experimental protocols that could better elucidate an EM's decomposition kinetics and thereby enable the bootstrapping of a mechanism's development and validation.

7. References

Bykov VI. A new synthesis of (*Z,E*)-undec-5-enoic acids, the sex pheromone of the varied carpet beetle Anthrenus verbasci. Russian Chemical Bulletin. 2004;53:2650–2652.

Clay AM, Banning JE. Investigation of acrylic-nitramine polymers as an energetic binder. DEVCOM Army Research Laboratory (US); 2020. Report No.: ARL-MR-1020.

Chen CC, Stone CP, McQuaid MJ, Veal JD. A detailed gas-phase finite-rate chemical kinetic mechanism for modeling the pyrolysis of 1,5,9-decatriene. Proceedings of the 44th JANNAF Propellant and Explosives Development and Characterization Subcommittee (PEDCS) Meeting; 2023a.

Chen CC, Stone CP, McQuaid MJ, Veal JD. Addendum to ARL-TR-9681, On modeling the pyrolysis of hydroxyl-terminated polybutadiene (HTPB)-type R45M at temperatures in the range 465–600 °C. DEVCOM Army Research Laboratory (US); 2023b. Report No.: ARL-TN-1155.

Chen CC, Stone CP, Cornell RE, McQuaid MJ. Addendum to ARL-TR-9869, On simulating the pyroprobe-induced pyrolysis of hydrocarbons with a model having a detailed finite-rate chemical kinetics mechanism: results for 1,5,9-decatriene. DEVCOM Army Research Laboratory (US); 2024 Jan. Report No.: ARL-TN-1191.

Fitch WL, Sauter AD. Calculation of relative electron impact total ionization cross sections for organic molecules. Anal Chem. 1983;55:832–835.

Kotlar AJ. A general approach for the reduction of chemical reaction mechanisms. I: methodology and application to MMH-RFNA. Proceedings of the 5th JANNAF Liquid Propulsion Subcommittee Meeting; 2010.

Li S, Petzold LR. Design of new DASPK for sensitivity analysis. University of California; 1999. Report No.: TRC99-28.

Lin Y-C, Cho J, Tompsett GA, Westmoreland PR, Huber GW. Kinetics and mechanism of cellulose pyrolysis. Journal of Physical Chemistry C. 2009;113:20097–20107.

Lutz AE, Kee RJ, Miller JA. SENKIN: a Fortran program for predicting homogeneous gas phase chemical kinetics with sensitivity analysis. Sandia National Laboratories (US); 1988. Report No.: SAND87-8248.

McQuaid MJ. The trial mechanism method for chemical kinetics mechanism reduction: an approach to generating reduced mechanisms with wider ranges

of applicability. Proceedings of the 7th JANNAF Liquid Propulsion Subcommittee Meeting; 2013a.

McQuaid MJ. Chemical kinetics mechanism reduction based on principal component analysis: development and testing of some new implementations. Army Research Laboratory (US); 2013b. Report No.: ARL-TR-6449.

McQuaid MJ. SENKIN3_PSB homogeneous reactor models: a primer. DEVCOM Army Research Laboratory (US); 2020a. Report No.: ARL-TR-8921.

McQuaid MJ. An opposed-flow diffusion flame simulation-based implementation of the trial mechanism method for chemical kinetics mechanism reduction: application to the San Diego mechanism for HTPB-air combustion modeling. DEVCOM Army Research Laboratory (US); 2020b. Report No.: ARL-TR-9032.

McQuaid MJ, Chen CC, Veals JD, Yeh IC. Detailed finite-rate chemical kinetics-based modeling of nitroglycerin in systems comprising liquid and gas phases. Proceedings of the 43rd JANNAF Propellant and Explosives Development and Characterization Subcommittee Meeting; 2021.

Pesce-Rodriguez RA, Chen CC, McQuaid MJ. Toward validating a framework for modeling high-throughput analytical techniques employed for energetic material screening. Part 1. Desorption/pyrolysis-gas-chromatography/mass spectrometry (D/P-GC/MS) results for 1,5,9-decatriene. DEVCOM Army Research Laboratory (US); 2023. Report No.: ARL-TN-1148.

Reynolds WC. The element potential method for chemical equilibrium analysis: implementation of the interactive program STANJAN. Stanford University; 1986.

Rozumov E, Caflin K, Liberatore-Moretti M. Iso-thermal gravimetric studies of double base propellants. Proceedings of the 42nd JANNAF Propellant and Explosives Development and Characterization Subcommittee Meeting; 2020.

Vermeire FH, De Bruycker R, Herbinet O, Carstensen HH, Battin-Leclerc F, Marin GB, Van Geem KM. Experimental and kinetic modeling study of the pyrolysis and oxidation of 1,5-hexadiene: the reactivity of allylic radicals and their role in the formation of aromatics. Fuel. 2017;208:779–790.

Zhou CW, Li Y, Burke U, Banyon C, Somers KP, Khan S, Hargis JW, Sikes T, Petersen EL, AlAbbad M, Farooq A, Pan Y, Zhang Y, Huang Z, Lopez J, Loparo Z, Vasu SS, Curran HJ. An experimental and chemical kinetic modeling study of 1,3-butadiene combustion: ignition delay time and laminar flame speed measurements. Combustion and Flame 2018;197:423–438.

Appendix. Estimating the Gas-Chromatography Detector Response Factors for Identified Molecules

Seeking to quantify the molar concentrations of organic molecules (k) in complex mixtures on the basis of the gas-chromatography (GC) ion currents (IC_k), Fitch and Sauter[1] proposed and evaluated a model predicated on the assumption that the only property of the molecules that needed to be known/estimated was their total ionization cross section (Q_k). That is, for n_k moles per unit volume (V), IC_k and n_k were related per

$$\frac{n_k}{V} = \frac{IC_k}{Q_k d I_e} \tag{A-1}$$

where d is the ionizing path length and I_e is the ionizing electron current. It thus follows that for a set of experiments in which V, d, and I_e are constants, Eq. A-1 reduces to

$$n_k = c' \frac{IC_k}{Q_k} \tag{A-2}$$

where c' is a constant. With certain caveats, this model retains currency.[2]

Because there were few published Q_k values at the time (and the situation is not much better today), Fitch and Sauter proposed and evaluated a scheme for estimating Q_k (in Å^2) based on the additivity of atomic cross sections,[1] namely

$$Q_k = b_0 + \sum_{m=1}^{M} b_m N_{k,m} \tag{A-3}$$

where M is the total number of atom types (m), b_m is the coefficient for type-m, and $N_{k,m}$ is the number of type-m atoms in k. Applying linear regression to 179 total ionization cross-section measurements for electron impact ionization at 70 and 75 eV, they parameterized two models for estimating Q_k for organic compounds comprising C, H, O, Cl, Br, I, F, and/or N atoms. One model classified C atoms according to their hybridization. The other did not.

The electron impact ionization value in the experiments performed by Pesce-Rodriguez et al.[3] was 70 eV. Therefore both models were applicable. However, given the exploratory nature of the investigation and our impression that the model that classified C atoms according to their hybridization produced correlations that were at best only slightly better than the one that did not, we employed the latter to

[1] Fitch WL, Sauter AD. Calculation of relative electron impact total ionization cross sections for organic molecules. Anal. Chem. 1983;55:832-835.

[2] Bose A, Westmoreland PR. Predicting total electron-ionization cross sections and GC-MS calibration factors using machine learning. Journal of Physical Chemistry A. 2020;124:10600–10615.

[3] Pesce-Rodriguez RA, Chen CC, McQuaid MJ. Toward validating a framework for modeling high-throughput analytical techniques employed for energetic material screening. Part 1. Desorption/pyrolysis-gas-chromatography/mass spectrometry (D/P-GC/MS) results for 1,5,9-decatriene. DEVCOM Army Research Laboratory (US); 2023. Report No.: ARL-TN-1148.

save time and effort. In that model, the only coefficients relevant to this effort were b_0 (0.082), b_C (1.43), and b_H (0.73).

Table A-1 compares the Q_k predictions produced by this model for (1) methane, ethylene, species observed following the pyroprobe-induced pyrolysis of 1,5,9-decatriene, and indene, to (2) the mean of measured values aggregated by Bose and Westmoreland.[2] (The model's prediction for 1,5,9-decatriene is included for reference.) The agreement between measured and predicted values for methane and the linear alkenes was excellent. The agreement between measured and predicted values for the four aromatic compounds (benzene, toluene, indene, naphthalene) was not nearly as good. However, the measured results for indene and naphthalene were each based on a single experiment and, given the similarity of their molecular structures, are difficult to reconcile with one another. As such, we were inclined to discount them.

Table A-1 Comparison of measured and model-predicted Q values

Molecule	N_C	N_H	Q(Å^2)	
			Model	Measured[a]
methane	1	4	4.4	4.6
ethylene	2	4	5.9	6.4
propene	3	6	8.8	9.0
1,3-butadiene	4	6	10.2	11.6
1-pentene	5	10	14.5	14.1
benzene	6	6	13.0	19.2
toluene	7	8	15.9	18.1
indene	9	8	18.8	27.3
naphthalene	10	8	20.2	11.4
1,5,9-decatriene	10	16	26.1	. . .

[a] As reported in supplemental information reported by Bose and Westmoreland.[2]

As for the predictions for benzene and toluene, since we would have been satisfied if the differences between abundances derived from measured IC_k values and model-predicted n_k values were less than a factor of 2, we considered the Q_k predictions produced by Fitch and Sauter's model sufficient for the purposes of the study. Indeed, to the extent that (1) our primary concern was resolving discrepancies between measurement-based and model-predicted abundances for methane and ethylene, and (2) the effort to rationalize all Q_k values would have been considerable and potentially introduced (our) biases, we opted to employ the Q_k predictions produced by Fitch and Sauter's model for all species.

List of Symbols, Abbreviations, and Acronyms

1,3-BD	1,3-butadiene
1,3-CHD	1,3-cyclohexadiene
1,3-CPD	1,3-cyclopentadiene
1,5-HD	1,5-hexadiene
ARL	Army Research Laboratory
ATOL	absolute tolerance
CAS	Chemical Abstracts Service
DEVCOM	US Army Combat Capabilities Development Command
D/P	desorption/pyrolysis
DTE	1,5,9-decatriene, $C_{10}H_{16}$
EM	energetic material
GC	gas chromatography
He	helium
HR	homogeneous reactor
HTPB	hydroxyl-terminated polybutadiene
ID	inner diameter
MEP	minimum energy path
MIT	Massachusetts Institute of Technology
ML	machine learning
MS	mass spectrometry
NMR	nuclear magnetic resonance
OFDF	opposed-flow diffusion flame
QM-ESM	quantum mechanics–based electronic structure method
RMG	Reaction Mechanism Generator
RTOL	relative tolerance
TMM	trial mechanism method

VOD	4-vinyl-1,7-octatriene
a_k^{GC}	gas-chromatography-based normalized abundance for species k
a_k^{pred}	model-predicted normalized abundance for species k
$a_k^{pred'}$	modified model-predicted normalized abundance for species k
b_m	coefficient for computing total ionization cross section
b_0	coefficient for computing total ionization cross section
c'	constant for scaling gas-chromatography-based normalized abundances
h_k	enthalpy per mole of species k
IC_k	chromatography ion current for species k
k	species index
K	total number of different species in the chemical kinetics mechanism
m_{prod}	mass of the products
m_{samp}	mass of the sample
MW_k	molecular weight of species k
n_{tube}	number of moles of gas in the tube
n_k	number of moles of species k in tube
n_k^{GC}	moles of species k derived from the chromatography ion current
$n_k^{t_0<t<t_f}$	number of moles of species k eluted from the tube while the heating coil is energized
$n_k^{t_f}$	number of moles of species k in the tube at the end of the heating cycle
$n_k^{t_0}$	number of moles of species k eluted from the tube prior to the heating coil being energized
n_k^{f}	number of moles of species k eluted from the tube plus number of moles of species k in the tube at t_f
$n_k^{f'}$	number of moles of species k eluted from the tube

$\dot{\omega}_k$	molar production rate of species k per unit volume
P	pressure
$\dot{q}$	rate of heat release
Q_k	total ionization cross section for species k
R	universal gas constant
t	time
t_f	time at which the heating coil is deenergized
t_0	time at which the heating coil is energized
T	temperature
T_{sp}	experiment set-point temperature
V	volume
X_k	mole fraction of species k

1 (PDF) DEFENSE TECHNICAL INFORMATION CTR DTIC OCA

1 (PDF) DEVCOM ARL FCDD RLB CI TECH LIB

12 (PDF) DEVCOM ARL FCDD RLA MG J ORLICKI FCDD RLA WA E BYRD B BARNES R PESCE-RODRIGUEZ FCDD RLA WC M MCQUAID C-C CHEN C STONE R CORNELL J LANSFORD M MINNICINO M NUSCA FCDD RLR A J CIEZAK

5 (PDF) NRL BT BOJKO T LOEGEL CJ PFUTZNER IV SCHWEIGERT A EPSHTEYN

2 (PDF) NAWS CHINA LAKE AR DEMKO JT ESSEL

1 (PDF) ONR C STOLTZ

1 (PDF) UNIV DAYTON RSRCH INST MJ DEWITT

1 (PDF) AFRL AEROSPACE RQ CASSELBERRY

4 (PDF) NTNL RENEWABLE ENERG LAB R MCCORMICK M RATCLIFFE G FIORONI J LUECKE

1 (PDF) UNIV CENTRAL FLORIDA S VASU

1 (PDF) MIT W GREEN

1 (PDF) BROWN UNIV F GOLDSMITH

1 (PDF) COLUMBIA UNIV M BURKE

1 (PDF) PURDUE UNIV B SAVOIE